Smell and Aftersmell: Fast Calcium Imaging Dynamics of Honey Bee Olfactory Coding

Marco Paoli[1], Antoine Wystrach[2], Brice Ronsin[2], Martin Giurfa[1,3]

[1] Neuroscience Paris-Seine – Institut de biologie Paris-Seine, Sorbonne Université, INSERM, CNRS, Paris, France

[2] Centre de Recherches sur la Cognition Animale, Centre de Biologie Intégrative, Université Paul Sabatier, CNRS, Toulouse, France

[3] Institut Universitaire de France (IUF), Paris, France

Abstract

Odour processing exhibits multiple parallels between vertebrate and invertebrate olfactory systems. Insects, in particular, have emerged as relevant models for olfactory studies because of the tractability of their olfactory circuits. Here, we used fast calcium imaging to track the activity of projection neurons in the honey bee antennal lobe (AL) during olfactory stimulation at high temporal resolution. We observed a heterogeneity of response profiles and an abundance of inhibitory activities, resulting in various response latencies and stimulus-specific post-odour neural signatures. Recorded calcium signals were fed to a mushroom body (MB) model constructed implementing the fundamental features of connectivity between olfactory projection neurons, Kenyon cells (KC), and MB output neurons (MBON). The model accounts for the increase of odorant discrimination in the MB compared to the AL and reveals the recruitment of two distinct KC populations that represent odorants and their aftersmell as two separate but temporally coherent neural objects. Finally, we showed that the learning-induced modulation of KC-to-MBON synapses can explain both the variations in associative learning scores across different conditioning protocols used in bees and the bees' response latency. Thus, it provides a simple explanation of how the time contingency between the stimulus and the reward can be encoded without the need for time tracking. This study broadens our understanding of olfactory coding and learning in honey bees. It demonstrates that a model based on simple MB connectivity rules and fed with real physiological data can explain fundamental aspects of odour processing and associative learning.

32 # Introduction

33 The logic of olfactory coding and learning has been extensively studied at the
34 behavioural and neural levels in various insect models **(Adam et al., 2022; Galizia, 2014;**
35 **Giurfa, 2015; Jefferis et al., 2007)**. Among them, the honey bee *Apis mellifera* has played a
36 pivotal role in our understanding of these processes due to its behavioural accessibility and
37 tractability of its nervous system. In bees, olfactory perception and learning have been typically
38 investigated using the proboscis extension reflex (PER) **(Giurfa, 2007; Menzel, 1999)**, a
39 protocol that relies on pairing a neutral olfactory stimulus (the conditioned stimulus or CS) with
40 a positive reinforcement of sugar solution (the unconditioned stimulus or US) **(Bitterman et**
41 **al., 1983; Giurfa and Sandoz, 2012; Takeda, 1961)**. In the classical version of PER
42 conditioning, the CS precedes and partially overlaps US presentation. This results in high
43 levels of specific memory for the conditioned odorant. Conversely, when the reward precedes
44 the stimulus (backward conditioning), no positive association can be established **(Felsenberg**
45 **et al., 2014; Hellstern et al., 1998)**. It also enables the study of more sophisticated cognitive
46 processes such as trace learning **(Paoli et al., 2023a; Szyszka et al., 2011)** and patterning
47 discrimination **(Deisig et al., 2001; Devaud et al., 2015)**. In the former, CS and US are not
48 overlapping but separated by a stimulus-free temporal gap, whereas in the latter, bees are
49 trained to respond in opposite ways to a two-odorant mixture compared to its individual
50 components **(Deisig et al., 2001; Devaud et al., 2015)**. Overall, the olfactory conditioning of
51 PER provides a robust read-out for investigating the dynamics of olfactory memory formation
52 **(Giurfa and Sandoz, 2012; Villar et al., 2020)** and olfactory perception **(Guerrieri et al.,**
53 **2005)**.

54 Our understanding of the neural processing subtending olfactory coding and learning
55 relies on decades of neuroanatomical and neurophysiological studies performed in honey bees
56 **(Paoli and Galizia, 2021)**. Olfactory processing starts at the peripheral level, when volatile
57 chemicals interact with the olfactory receptors expressed on the dendritic membrane of the

58 olfactory sensory neurons (OSNs). The biochemical nature of odorant-receptor interactions
59 allows for a certain molecule to bind to multiple receptors with different affinities, resulting in
60 the activation of an OSNs sub-population with odorant-specific response intensities and
61 latencies **(Münch and Galizia, 2016)**. Olfactory sensory neurons innervate the first olfactory
62 processing centre, the antennal lobe (AL), where the neurons expressing the same olfactory
63 receptor converge onto one of ~160 glomeruli, the anatomical and functional units of the AL
64 **(Flanagan and Mercer, 1989)**. Thus, odorant detection results in the stimulus-specific
65 activation of a subset of glomeruli, creating a stereotypical map of odour-induced glomerular
66 responses **(Galizia et al., 1999; Sachse et al., 1999)**. The signal processed in the AL is
67 forwarded by ~800 output neurons - the projection neurons (PNs) - to higher-order brain
68 centres: the mushroom bodies (MBs), central, paired structures dedicated to multisensory
69 integration, memory storage and retrieval **(Heisenberg, 2003; Stopfer, 2014)**, and the lateral
70 horn of the protocerebrum, a diffuse bilateral structure involved in valence coding of odorants
71 **(Jeanne et al., 2018; Roussel et al., 2014; Strutz et al., 2014)**. The MB architecture is defined
72 by the layout of its ~185 000 intrinsic neurons, the Kenyon cells (KCs). Each KC extends its
73 dendritic arborisation within the MB input regions, termed the calyces, where it receives input
74 from multiple PNs, and projects its axon to the MB output region, termed the pedunculus,
75 where it bifurcates into the vertical (α and γ) and the medial (β) lobes **(Mobbs, 1982;**
76 **Strausfeld, 2002)**. Kenyon cells integrate, among others, the excitatory input of olfactory PNs
77 and the inhibitory input of recurrent GABAergic feedback neurons **(Ganeshina and Menzel,**
78 **2001; Grünewald, 1999; Rybak and Menzel, 1993; Zwaka et al., 2018)**. The latter plays a
79 critical role in shaping KCs olfactory responsiveness and maintaining a sparse output over a
80 wide range of odorants and concentrations **(Papadopoulou et al., 2011; Stopfer, 2014)**.
81 Antennal lobe, mushroom body and lateral horn are innervated by the VUMmx1 neuron
82 **(Hammer, 1993)**, an unpaired octopaminergic neuron conveying appetitive reward-related
83 information to the olfactory circuit and mediating reward-based olfactory memory formation.
84 The activity in the Kenyon cells is integrated by MB output neurons (MBONs). These neurons
85 exhibit which show learning-related plasticity and provide valence-loaded information to pre-

86 motor areas **(Aso et al., 2014a; Okada et al., 2007; Schmalz et al., 2022; Strube-Bloss and**
87 **Rössler, 2018)**.

88 The neural representation of odorants in the AL has been extensively described by
89 means of functional calcium imaging **(Paoli and Haase, 2018)**. *In vivo* imaging allowed
90 observing that each stimulus is represented with a specific pattern of excitatory and inhibitory
91 responses across the glomeruli of the AL, **(Galizia et al., 1999; Sachse and Galizia, 2002;**
92 **Sachse et al., 1999)**, and that perceptually similar odorants elicit similar glomerular response
93 patterns **(Guerrieri et al., 2005)**. Calcium imaging of AL activity has been typically conducted
94 at low temporal resolutions (~100-200 ms) **(Locatelli et al., 2016; Mertes et al., 2021;**
95 **Nouvian et al., 2018; Sachse and Galizia, 2003)**. This is partially justified by the slow
96 dynamics of fluorescent calcium sensors, which resulted - in general - in the compression of
97 olfactory representation into a spatial vector of glomerular response intensity, with a
98 concomitant loss of information on neural response dynamics. While calcium signal decay is
99 relatively slow (>100 ms), its onset is fast (<10 ms) **(Helassa et al., 2015; Moreaux and**
100 **Laurent, 2007)**, and provides the possibility for investigating parameters such as glomerular
101 response latency **(Junek et al., 2010; Paoli et al., 2018)**, signal frequency components **(Paoli**
102 **et al., 2016)** and interglomerular information transfer **(Chen et al., 2023; Paoli et al., 2023b)**.
103 In this study, we significantly improved the temporal resolution of calcium imaging recordings
104 of olfactory neurons in the bee brain by means of a resonant scanning multiphoton microscope.
105 This allowed us to record calcium activity at a <10-ms resolution, preserving temporal
106 information of the olfactory code and yielding a more realistic representation of odour
107 trajectories in the AL. First, we observed that odour representation changes dynamically during
108 and after an olfactory stimulation, resulting in specific odour and after-odour images. Then, we
109 showed that most glomerular response profiles presented an inhibitory component, suggesting
110 that glomerular activity is strongly shaped by local inhibition, with only a minor influence - if any
111 - of local excitatory interneurons.

112 Calcium imaging analysis was combined with a modelling approach to investigate how
113 odorant representation evolves from the AL to the MB. Electrophysiology experiments have

provided insight on the phasic and sparse activity of Kenyon cells as well as into its oscillatory nature **(Laurent and Davidowitz, 1994; Perez-Orive et al., 2002; Stopfer, 2014)**. However, the unavailability of an imaging method allowing the visualisation of olfactory coding in a KC ensemble prevented us from further understanding how odorants are represented within the MB, *e.g.* how the neural representation of an odorant is transformed from the AL to the MB or to what extent the similarity among odorant representation is maintained in the KC space. One way to address these questions is by using neural network models constructed *via* the abstraction of common features of MBs across insect species (*e.g.* fruit fly, locust, honey bee) to reproduce cognitive tasks such as stimulus discrimination or learning. Models can be built by simulating multiple neurons interacting with each other according to physiological rules such as the dynamics of action potentials or Hebbian synaptic plasticity **(Eschbach et al., 2020; Finelli et al., 2008; Gkanias et al., 2022; Huerta et al., 2004; Smith et al., 2008)**. Other models simulate the MB neural network by considering the statistics of connectivity within the neuropil, *e.g.* the ratio of PNs to KCs, the average number of synaptic connections, the neuronal firing rate **(Ardin et al., 2016; Buehlmann et al., 2020; Le Moël et al., 2019; Peng and Chittka, 2017; Springer and Nawrot, 2021; Wystrach, 2023)**. Here, we followed the second approach and built a simplified but realistic neural network model of the MB based on the neuroanatomical and functional properties of the insect's olfactory circuit. The model comprises three layers of neurons: (1) a MB input layer to provide the model experimentally acquired time-series of PN activity; (2) a MB intrinsic layer, where the input signal is distributed to a population of modelled KCs based on neuroanatomical and physiological data; (3) a MB output layer, where one appetitive MB output neuron (MBON) receives input from the KC layer and can be subject to learning-induced plasticity. Generally, the input for this type of model is simulated based on the spatial and temporal statistics of the odour-induced glomerular activity **(Eschbach et al., 2020; Finelli et al., 2008; Gkanias et al., 2022; Huerta et al., 2004; Le Moël and Wystrach, 2020; Peng and Chittka, 2017; Smith et al., 2008; Springer and Nawrot, 2021)**. In this case, we fed the model with the time series of the PN responses recorded via *in vivo* calcium imaging analysis from multiple individuals exposed to three

142 different odorants at the MB working frequency of 20 Hz **(Cassenaer and Laurent, 2007;**
143 **Laurent and Naraghi, 1994)**.
144 Here, we show that an MB neural network model based solely on three simple
145 connectivity rules abstracted from insect studies - sparse connectivity, feedback inhibition, and
146 learning-induced synaptic modulation - is sufficient to explain fundamental MB processing
147 features such as improved olfactory discrimination and associative learning. The model also
148 predicts that the presence of post-stimulus inhibitory and excitatory activity leads to the
149 recruitment of a second pool of KC, resulting in a distinct after-odour representation in the MB.
150 Additionally, the model's performance in appetitive learning and across-stimuli generalisation
151 was coherent with empirical measurements obtained from behavioural protocols. Finally, using
152 real physiological datasets as input, we showed that such a model is robust to noise and
153 biological variability across multiple stimulus repetitions.

154 Results

155 Response dynamics of projection neurons in high-temporal resolution

156 Antennal lobe PNs of eight bees were back-filled with the calcium sensor Fura-2 **(Paoli**
157 **and Haase, 2018; Sachse and Galizia, 2002)** to measure odour-induced glomerular activity
158 of (~25 glomeruli/AL) (**Fig. 1A**). Calcium signal was recorded upon stimulation with two
159 monomolecular odorants (1-hexanol, 1-heptanol) and a complex fragrance (peppermint oil) on
160 a 5s/25s ON/OFF conformation for 20 trials (**Fig. 1B-D**). Fast calcium imaging revealed the
161 high variability of odorant-elicited glomerular response profiles.
162 First, we assessed the stability of odorant representations across time and trials given
163 the duration of each imaging session (30 min) and the multiple stimulus repetitions. For each
164 individual, we calculated the Pearson's correlation coefficients across pairs of trials of the
165 glomerular response vectors before, during and after olfactory stimulation. **Figure 1E** shows

166 that across-trial correlation is elevated during odour arrival and still ~0.5 after stimulus
167 termination. This shows that, in our experimental conditions, odour coding was stable
168 throughout the entire imaging period.

169 All odorant response traces were pooled together (**Fig. 1F**) and clustered according to
170 their direction with respect to the pre-stimulus baseline (*i.e.*, excitatory or inhibitory) and
171 duration (**Fig. 2,** see **Materials and Methods**), allowing for a statistical description of
172 glomerular responses across individuals and odorants, and for the identification of classes of
173 recurrent profiles (**Fig. 2A,B**). The most common profiles comprised inhibitory (group 1) and
174 excitatory (group 4) responses lasting the entire olfactory stimulations and terminating after
175 odour offset. In some cases, they could result in prolonged inhibition (group 2) or excitation
176 (group 6) lasting after stimulus offset or could be followed by a post-stimulus excitatory (group
177 3) or inhibitory activity (group 5). Approximately 15% of responses consisted of short phasic
178 excitation followed by prompt signal termination (group 7) or even by an inhibitory response
179 (group 8). About 15% of all recorded glomerular traces showed no detectable odorant-induced
180 activity (group 9). Of all traces, 48% were excitatory, 37% inhibitory, and 15% unresponsive
181 (**Fig. 2C,D**). Moreover, 251 glomerular responses out of 546 (46%) displayed an inhibitory
182 component either during or after olfactory stimulation.

183 The heterogeneity of PNs response profiles could be due to the diversified temporal
184 pattern of the ONSs input **(Kim et al., 2023)** and to second-order processing mediated by
185 lateral connections within the AL **(Girardin et al., 2013; Krofczik et al., 2009)**. We assessed
186 the contribution of these two components by measuring the latency of excitatory and inhibitory
187 glomerular responses (*i.e.* the timepoint *t* at which a response profile exceeds the threshold of
188 one standard deviation from the mean pre-stimulus activity). **Figure 2E** shows that excitatory
189 responses (groups 4 to 8) all share a similar onset (313 ± 22 ms, n = 263), which is shorter
190 than that of inhibitory profiles (groups 1 to 3; 351 ± 47 ms, n = 201) (Kruskal-Wallis test, p<0.05,
191 Tukey-Kramer multiple comparison correction). Moreover, the latency of short excitatory
192 responses' termination (groups 7 and 8; 346 ± 47 ms, n = 60) is coherent with the onset of
193 inhibitory profiles. These findings indicate that odour representation in the AL is shaped initially

194 by the excitatory input delivered by the OSNs and reshaped - approx. 40 ms later - by local
195 inhibition. Such an olfactory tuning is different from what is proposed in *Drosophila*, where both
196 excitatory and inhibitory local neurons contribute to moulding the neural correlate of an
197 olfactory input **(Chou et al., 2010; Olsen et al., 2007)**.

198 A mushroom body neural network model: Key principles

199 We constructed a simple but realistic MB neural network model based on the known
200 connectivity of this structure in the insect brain. The model architecture relies on three main
201 principles (**Fig. 3**): First, in each brain hemisphere, ~800 AL projection neurons (PNs) diverge
202 onto ~185,000 KCs **(Strausfeld, 2002)**. Neuroanatomical studies in bees **(Szyszka et al.,**
203 **2005)** and flies **(Ashok Litwin-Kumar et al., 2017; Caron et al., 2013)** suggest that each KC
204 is randomly innervated by approx. 7-10 PNs. Thus, we generated a MB network where ~25
205 PNs (*i.e.*, the average number of glomeruli imaged during a calcium imaging experiment)
206 diverge onto 1000 KCs, with each KC being innervated by ~8 PNs. Second, recurrent inhibitory
207 neurons such as the A3 feedback neurons in the bee **(Mobbs, 1982; Rybak and Menzel,**
208 **1993; Szyszka et al., 2005; Zwaka et al., 2018)**, the APL neuron in fly **(Lin et al., 2014)**, and
209 the giant GABAergic neuron in the locust **(Papadopoulou et al., 2011)**, modulate MB KCs
210 firing rate so that less than 20% of KCs are active upon olfactory stimulation, and only ~5%
211 are stimulus-specific **(Honegger et al., 2011; Turner et al., 2008)**. Hence, we enriched the
212 model with a winner-takes-it-all feedback inhibition mechanism by forcing that only 10% of KCs
213 receiving the largest summed input generate an action potential. Third, as in bees and locusts,
214 MB have a 20-Hz oscillatory cycle **(Cassenaer and Laurent, 2007; Laurent and Naraghi,**
215 **1994; Popov and Szyszka, 2020)**, we fed the model with experimentally recorded calcium
216 signals resampled at a 20 Hz-sampling frequency. This approach allowed testing if a simple
217 neural architecture - so far challenged with simulated datasets **(Ardin et al., 2016; Buehlmann**
218 **et al., 2020; Peng and Chittka, 2017)** - could be used for understanding how real odour

219 activity recorded at the level of PNs is transformed in the MB, and if the rules governing the
220 model were sufficient to support appetitive olfactory conditioning.

221 Model input and output: Simulating olfactory coding in the mushroom body

222 For each recorded individual AL (n = 8), an MB simulation was generated and fed with
223 the time series of the recorded glomerular activity obtained for that individual. Thus, for each
224 odorant and individual, we simulated the time course of the firing of a virtual KC ensemble
225 (**Fig. 4A**). The analysis of KC population turnover (**Fig. 4B**) showed that, before odorant onset,
226 the population varies randomly between adjacent time points while it stabilises during olfactory
227 stimulation, with a turnover rate of ~10%. The dynamics of KC recruitment across bees and
228 odorants (**Fig. 4C**) indicates that two odorant-specific sets of cells are recruited during an
229 olfactory stimulation: the first one at stimulus onset, the second one at odour termination (see
230 **Fig 4C**, t = 5 s). Both populations are rather stable, with a turnover rate below the pre-stimulus
231 baseline for up to 15 s after stimulus offset (turnover $\text{rate}_{\text{pre-stim}}$ = 0.61 ± 0.14; turnover $\text{rate}_{\text{ON_0-}}$
232 $_{\text{5s}}$ = 0.17 ± 0.05; turnover $\text{rate}_{\text{OFF_5-10s}}$ = 0.25 ± 0.04; turnover $\text{rate}_{\text{OFF_10-15s}}$ = 0.33 ± 0.08).
233 Correlation analysis of stimulus-induced responses (**Fig. 5D**,**E**) showed a high correlation of
234 neural activity across time points during olfactory stimulation and during the post-odour window
235 both in the recorded PN population and in the simulated KCs. This indicates that the neural
236 representation of an odorant is sufficiently stable to provide a neural image, which is coherent
237 with itself during a 5-s stimulation window and during a ~10-s post-stimulation window.
238 Furthermore, the across-odorants correlation is rather high in the PN space (Pearson's
239 correlation coefficient, r = 0.4), but proximal to zero in the KC space, supporting the notion that
240 the MB network increases stimulus discriminability, not only during but also after odour offset.
241 To further corroborate this idea, we compared the temporal relative trajectories obtained
242 for the three odorants in the measured PN space and in the modelled KC space (**Fig. 4F**). In
243 both cases, response trajectories diverged at stimulus onset and returned to the centre of
244 space after stimulus termination. However, the principal component analysis showed that

245 odorants are better separated from each other and that they remained separated for a longer
246 time in the KC space compared to the PN space. This indicates improved and prolonged
247 stimulus discriminability in the MB with respect to the AL (**Fig. S1**).

248 We next investigated the discriminatory power of the system across a larger set of odour
249 response profiles. For this, we pooled together all response profiles acquired during the
250 calcium imaging analysis (**Fig. 1F**) and we artificially combined them to simulate 100 odorant
251 response vectors, each comprising 30 different glomerular profiles (see **Methods**). Using
252 these artificially combined odorant response profiles, we simulated the relative KC response
253 time series and measured the correlation across all response vectors in the PNs (experimental
254 data) and KCs spaces (modelled data) (**Fig. 4G**). Notably, while response vectors calculated
255 from PN data were highly correlated ($r = 0.71 \pm 0.08$), such a correlation significantly decreased
256 in the modelled KC space ($r = 0.52 \pm 0.10$; Student's *t*-test between *r* distributions of PN and
257 KC data: $p \approx 0$, $n = 4774$), indicating that the signal transformation operated by the proposed
258 MB neural architecture induces a strong decorrelation among odour signatures.

259 Overall, the proposed MB network can process experimentally acquired input data and
260 produce physiologically plausible KC response patterns coherent with *in vivo* KC activity
261 measurements **(Lüdke et al., 2018)**. Moreover, it accounts for the expansion of the coding
262 space from the AL to the MB **(Lin et al., 2014; Papadopoulou et al., 2011; Stopfer, 2014)**,
263 enhancing inter-stimuli decorrelation and confirming previous theoretical works based on
264 artificial datasets **(Olshausen and Field, 2004; Peng and Chittka, 2017)**. Importantly, these
265 emergent properties of the model architecture are based on the known neuroanatomy and
266 physiology of the insect brain and have been obtained without any optimisation aiming at
267 reproducing specific features of olfactory coding.

268 The neural network model predicts appetitive behaviour

269 Appetitive classical conditioning relies on the coincidental activation of the neural
270 elements representing the conditioned stimulus (CS) and the unconditioned stimulus (US). The

271 latter is mediated by various neuromodulators, such as specific dopaminergic, as shown in the
272 fly **(Burke et al., 2012; Liu et al., 2012)**, or octopaminergic neurons, as demonstrated in the
273 honey bee **(Hammer, 1993)**.

274 The coincidental activation of CS and US neural elements induces plastic modulations
275 in the MB output neurons (MBONs) **(Hige et al., 2015; Okada et al., 2007; Owald et al.,**
276 **2015)**. Here, we assessed if the proposed MB model could reproduce empirical measurements
277 of appetitive learning by introducing a time window, during which the weights of the recruited
278 KC-to-MBON synapses could be downregulated from 1 to 0 **(Ardin et al., 2016)**. This rule
279 reflects MBON learning-induced plasticity, according to which they display a broadly tuned
280 response, which is reduced in presence of a learned stimulus **(Amin and Lin, 2019; Aso et**
281 **al., 2014a; Aso et al., 2014b; Cognigni et al., 2018; Cohn et al., 2015; Hige et al., 2015;**
282 **Lyutova et al., 2019; Okada et al., 2007; Owald et al., 2015)**. To implement such a rule, we
283 introduce a synaptic plasticity threshold (*spt*) parameter, which defines the number of firing
284 events of a given KC upon which its synaptic output weight is reduced from 1 to 0. In other
285 words, it determines how active a synapse should be during the learning window before being
286 switched off.

287 It is well known that the inter-stimulus interval (ISI) - *i.e.* the time elapsed from CS to US
288 onsets - can influence the efficiency of Pavlovian learning **(Domjan, 2015; Holland, 1980)**.
289 The calcium signal dynamics and modelling analysis presented here (**Fig. 4A-F**) suggest that
290 such an ISI-dependent effect is the consequence of the strong temporal dynamics of the
291 odorant neural representation. As the neural representation of the CS changes in time, a
292 reward system recruited at different time points will interact with a different population of CS-
293 recruited KCs. Because learning results from the coincidental activation of CS and US
294 elements **(Pavlov, 1927)**, an individual should respond to the different time points of an
295 olfactory stimulation with different strengths, depending on the US arrival time experienced
296 during conditioning. To test this hypothesis, learning-related MBON plasticity was modelled for
297 three different CS/US temporal contingencies reflecting three conditioning paradigms, well-
298 studied in honey bee **(Giurfa and Sandoz, 2012)** (**Fig. 5A**). Having a fixed CS stimulation

299 interval from t = 0 to 5 s, and a learning window (US) of 3 s, we simulated MBON learning with
300 three different ISIs. *Backward* pairing occurred when the US initiated at t = -2 s (*i.e.* 2 s before
301 CS onset), *early* pairing when it started at t = 1 s (*1 s* after CS onset), and *delay* pairing when
302 it started at t = 4 s (4 s after CS onset). First, we trained the model with the experimental PN
303 response profile recorded for either 1-hexanol or peppermint oil (see **Fig. 1**). One odorant was
304 used as CS and the other as a novel odorant to test the specificity of the learning obtained
305 under these experimental conditions. After learning, we modelled the MBON action potential
306 (AP) probability upon the presentation of the CS (*e.g.* 1-hexanol) and the novel odorant (*e.g.*
307 peppermint) and repeated this operation for the response profiles of all individuals. To account
308 for the biological variability in the neural activities elicited by repetitions of the same stimulus,
309 learning was assessed against the KC response profiles resulting from five CS and five novel
310 odorant presentations, which were not included in the training dataset. As expected, we found
311 that a trained MBON showed a larger decrease in firing probability when presented with the
312 CS than with the unfamiliar stimulus, demonstrating learning (**Fig. 5B** and **C**). Interestingly, the
313 model predicts weak learning in the case of *backward* pairing - that is when US and CS are
314 partially overlapping, but the US begins before the CS - whereas both *early* and *delay*
315 conditioning produced a CS-specific down-regulation of MBON firing probability. The model
316 also predicts that high synaptic plasticity sensitivity (low *spt* values) facilitates non-specific
317 learning, resulting in a strong generalisation effect. Conversely, MBON plasticity under high
318 *spt* values requires a robust and stable KC activation, a situation that is not compatible with a
319 learning interval that is only partially overlapping with the stimulation window (note that
320 measurements are provided at 20 Hz, and in this context, a *spt* = 40 requires a synapse to be
321 activated during two whole seconds - although not continuously - to be switched off) (**Fig. S2**).
322 Stimulus representation is dynamic (see **Fig. 1** and **2**). Hence, our model predicts that
323 an MBON exposed to an *early* protocol should learn to identify the early components of the
324 stimulus neural signature. Indeed, the model shows that the learned response (a down-
325 regulation of MBON firing probability) occurs earlier in the *early* than in the *delay* contingency
326 (Wilcoxon test for non-parametric paired data, $p < 0.001$; $n = 16$) and with lower response

327 latency variability (Barlett's test, $p < 0.011$) (**Fig. 5D**). To test the model's predictions, we
328 measured the timing of real behavioural responses (*i.e.* the proboscis extension) of honey
329 bees trained under the same CS/US conditions and tested 1 hour later with the CS and a novel
330 odorant. Because the model's predictions were generated based on the odour response maps
331 elicited in the AL by 1-hexanol and peppermint oil, the same odorants were used for the
332 behavioural experiments. In agreement with the model's predictions and previous reports
333 **(Felsenberg et al., 2014)**, *backward* conditioning led to scarce and unspecific responses (**Fig.**
334 **5E**). In contrast, positive ISIs of 1 or 4 seconds (*early* and *delay* protocols) induced specific
335 memory formation (McNemar test, $p_{backward}$ = n.s., $p_{early} = 0.003$, $p_{late} = 0.004$), with ~90 to 70%
336 of the trained bees showing conditioned responses to the CS and ~40% showing a generalised
337 response to the unfamiliar stimulus during the test. Video tracking of the proboscis extension
338 response showed that bees receiving the reward 1 s after CS onset extended the proboscis
339 earlier and with less variability than those that received the reward towards the end of CS
340 delivery (Kruskal-Wallis test, $p = 0.036$; Barlett's test for data variance comparison, $p = 5e10^{-}$
341 ^{6}; $n_{early} = 26$, $n_{delay} = 20$) (**Fig. 5F**).

342 ## Discussion

343 Our results show that a simple but biologically realistic MB neural network model
344 simulating essential aspects of MB connectivity can process real neurophysiological input and
345 generate robust predictions that agree with empirical observations. Our model was fed with
346 experimental PN responses acquired at high temporal resolution **(Bestea et al., 2022; Paoli**
347 **and Haase, 2018)**. This approach provided a better description of the temporal dynamics of
348 olfactory coding and a more realistic modelling of odour signal transformation and learning.

349 Olfactory trajectories in the glomerular space are shaped by local inhibition

350 Because of the high temporal resolution of the functional imaging recordings, we could
351 reliably measure odorant-induced latencies of excitatory and inhibitory PN responses.
352 Excitatory responses occurred earlier than inhibitory ones and exhibited a smaller temporal
353 variability. This suggests that excitation of PNs occurs in a single wave upon cholinergic input
354 from the OSNs to the glomeruli of the antennal lobe, with a minor contribution - if any - of
355 second-order excitatory local interneurons within the AL, which have been reported for
356 *Drosophila* **(Chou et al., 2010; Olsen et al., 2007)** but so far not for honey bees **(Girardin et**
357 **al., 2013; Krofczik et al., 2009; Schäfer and Bicker, 1986)**. This finding also advocates that
358 odour responses of OSNs may not display onset-latency variability as shown in the locusts
359 **(Kim et al., 2023)**. On the other hand, inhibitory PN responses and the termination of early
360 excitatory PN responses occurred within the same time window, approx. 40 ms after the onset
361 of excitatory responses, suggesting that lateral inhibition within the AL is responsible for
362 triggering PN inhibition and terminating early excitatory responses (see **Fig. 2**, groups 7 and
363 8). This is consistent with a significant presence of GABAergic local interneurons in the AL
364 **(Schäfer and Bicker, 1986)**, which reshape the olfactory message conveyed to higher-order
365 brain structures such as the MBs and the lateral horn **(Paoli and Galizia, 2021)**. Notably, we
366 observed that almost 50% of PN responses recorded contain an inhibitory component (see
367 **Fig. 2A**, groups 1-3,5,7,8), underlining the dominant role of inhibitory AL interneurons in
368 shaping odour trajectories in the glomerular space. These observations are in contrast with
369 previous calcium imaging analyses, where only 2-10% of responses had an inhibitory nature
370 **(Krofczik et al., 2009; Szyszka et al., 2005)**, but coherent with electrophysiological recordings
371 showing a rich response diversity and prominence of inhibitory activity **(Wilson et al., 2004)**.
372 Differently from *Drosophila*, where both local inhibitory and excitatory interneurons contribute
373 to the olfactory tuning **(Chou et al., 2010; Huang et al., 2010; Shang et al., 2007; Yaksi and**
374 **Wilson, 2010)**, our analysis indicates that, in the honey bee AL, glomerular responses are
375 modulated mainly by a local inhibitory network. This conclusion is supported by a previous

376 study showing that pharmacological activation of a single glomerulus by topical acetylcholine
377 application provokes inhibitory but not excitatory responses in other glomeruli **(Girardin et al.,**
378 **2013)**. Indeed, while the presence of excitatory local interneurons have been predicted
379 **(Malaka et al., 1995)**, such prediction has never been supported by experimental evidence.
380 Overall, these findings highlight possible differences between the ALs of bees and fruit
381 flies regarding the nature of the local interneuron populations modulating glomerular activity.
382 Thus, they cast caution in prioritising a single species as a representative general model of
383 insect olfaction.

384 ## Smell and aftersmell: An odorant-specific afterimage

385 Almost 50% of all PN responses in our database displayed either a prolonged post-
386 stimulus activity (see **Fig. 2**, groups 2 and 6) or a change in response direction after stimulus
387 termination (groups 3, 5, 7, 8). This results in the recruitment of an offset-specific population
388 of KC - both in our model and in the literature **(Ito et al., 2008; Lüdke et al., 2018)** - that
389 creates a neural image of the post-odour in the MB. Thus, the post-odour representation is
390 different from the neural image of the odorant itself and provides a stable, slowly decaying
391 after-image, which is stimulus-specific and temporally associated with the neural correlate of
392 the odorant itself. This is in agreement with the analysis conducted by Patterson *et al.*
393 **(Patterson et al., 2013)** on the olfactory representation in M/T cells in mice, which shows that
394 the post-odorant activity is rather conserved and stimulus-specific even across concentrations
395 and for about a 10-s window. Our modelling analysis predicts that the after-stimulus signature
396 of an odorant is more distinct and stable across time in the MB than in the AL (**Fig. S1**). This
397 could occur because the activity across the KC population is normalised by the MB feedback
398 neurons operating a gain control, which stabilises odorant-responses signature in the MB -
399 including the post-odorant activity - while the input signal in the PN is fading.
400 The existence of a post-odour signature has important implications for understanding the
401 neurobiological basis of trace learning **(Dylla et al., 2013; Paoli et al., 2023a)**, a conditioning
402 protocol in which a stimulus-free time window separates CS and US. Previous studies reported

403 that an odorant cannot be predicted by its post-odour signature **(Lüdke et al., 2018; Szyszka**
404 **et al., 2011)**. Nevertheless, the post-odour image is stimulus-specific and always temporally
405 contiguous to the neural representation of the odorant itself. As shown in previous studies
406 **(Galili et al., 2011; Lüdke et al., 2018; Patterson et al., 2013; Szyszka et al., 2011)**, the
407 neural activity associated with the OFF response is stimulus-specific and reproducible,
408 suggesting that the post-odour could be physiologically similar to the onset of a second odorant
409 (in the same way as the back-taste of wine could remind us of an unrelated ingredient). If so,
410 the odour/post-odour pattern could be processed as an individual neural object, effectively
411 extending the duration of the nominal, conditioned odour. Interestingly, the duration of the post-
412 odour neural signature reported by us and by previous studies **(Galili et al., 2011; Patterson**
413 **et al., 2013; Szyszka et al., 2011)** is about 10 to 15 s. As such, it is compatible with the
414 duration of the CS/US gap in trace learning experiments **(Galili et al., 2011; Paoli et al.,**
415 **2023a; Szyszka et al., 2011)**, suggesting the possibility of its implication in this form of
416 learning.

417 Mushroom body modelling predicts associative learning scores and response latency for
418 different conditioning protocols

419 To investigate if the proposed neural network model explains the temporal features of
420 associative learning, we simulated CS delivery by feeding the model with experimental PN
421 calcium imaging time series and applied a learning rule based on the downregulation of
422 recurrently recruited synapses in the MB. A learning time window of 3 s was defined according
423 to three well-studied protocols for associative conditioning, which correspond to three different
424 ISI situations (-2s, +1s and +4s) **(Bitterman et al., 1983; Giurfa and Sandoz, 2012)**. A
425 simulation of the action potential probability of an MBON after olfactory conditioning revealed
426 that differentiation between the CS and a novel odorant was observable whenever the CS
427 anticipated the US (ISIs of +1s and +4s) but less successful in the *backward* protocol (IS of -
428 2s). Generalisation errors were also observed in a similar way as in behavioural experiments.
429 Notably, in this study, we adopted a backward contingency with a 1-second overlap between

430 the US and the CS (**Fig. 5A**). This differs from the more traditional configuration, where the
431 CS is delivered after US termination, that is, without any temporal overlap. In this case, the
432 model would predict no learning at all, as observed in honey bee behavioural experiments
433 **(Felsenberg et al., 2014; Hellstern et al., 1998)**. Hence, we tested the model's prediction in
434 the form of backward conditioning where US and CS are partially overlapping. In this case, the
435 model predicts a weak appetitive association (see **Fig. 5B,C,E**). This result is coherent with a
436 previous behavioural report, where bees subject to a similar protocol showed a weak response
437 to the conditioned odorant **(Felsenberg et al., 2014)**. In the early and delay configurations, a
438 CS-specific associative memory was formed, both in the model (**Fig. 5C**) and in the
439 behavioural tests (**Fig. 5E**). However, the model predicts a difference in response latency and
440 latency variability depending on relative CS/US arrival (ISI of +1 or +4 s): a learning window
441 placed closer to stimulus onset (*early* protocol) resulted in early and temporally precise MBON
442 responses, whereas a delayed learning window produced a similar learning score, but with
443 higher response latencies and temporal uncertainty

444 Experimental results based on the same odorants that were fed to the model confirmed
445 the model's predictions. They showed that the two forward CS/US contingencies (*i.e. early* and
446 delay protocols, with the CS anticipating the US) yielded comparable results in terms of
447 learning score and CS-specificity while differing in terms of CS latency and precision (**Fig. 5C-**
448 **F**). These observations support the idea that associative learning occurs upon coincident
449 detection of the CS and US neural elements. In fact, because the CS neural representation
450 changes dynamically during the olfactory stimulation, a positive association with the initial
451 odour signature will trigger an earlier and temporally precise conditioned response.
452 Conversely, the association with the later part of the olfactory signature will elicit a delayed
453 response with greater temporal variability.

Encoding time without encoding time

It has been reported that mammals can encode the CS/US interval time, allowing them to modulate the latency of a conditioned response **(Kirkpatrick and Balsam, 2016)**. However, it is still unclear whether also smaller, less complex insect brains are capable of time tracking. Previous studies have shown that the duration of the inter-stimulus interval experienced during learning can influence the conditioned response's latency in bumble bees **(Boisvert and Sherry, 2006)** and honey bees **(Szyszka et al., 2011)**. Both studies indicate that bees trained with a longer ISI exhibited a larger latency in their response to the conditioned stimulus. This provided clear evidence that CS-related information can modulate response timing. However, the appetitive response largely anticipated the expected reward time, and a clear interpretation of time tracking in insect brains is still missing

Our model shows that this time contingency is naturally encoded, simply because the olfactory representation in the KCs evolves through time in a deterministic fashion. Thus, what is learnt at the time of the US presentation is the KC configuration of the CS at this particular time. In other words, the MBON learns which subpopulation of KC is active during reward arrival, rather than the expected reward time. Interestingly, because the KC representation of the CS does not evolve linearly with time (**Fig. 4A-C**), the CS/US time contingency is not encoded perfectly. Remarkably, the model captures the experimental measurements of the proboscis response latency in bees, which indeed tend to respond earlier than the expected reward (**Fig. 5D,F**).

As often in insect research, heuristics can provide simple solutions to apparently complex cognitive problems. In this case, a mechanism based on the temporal dynamics of the conditioned stimulus, explains the bees' systematic errors at encoding proper CS/US contingency. Whether, in addition to this process, other mechanisms enable bees to track time contingencies remains to be seen.

Conclusive remarks

In this study, we adopted a fast calcium imaging approach to investigate the dynamical representation of odorants in the antennal lobe. Our findings revealed that about 50% of glomerular responses had an inhibitory component and that local inhibition played a crucial role in shaping the initial PN activity and defining odour trajectories in the glomerular space. We observed that half of the PN response profiles prolonged their activity or changed response direction after stimulus termination, generating a stable, odorant-specific after-smell. Although the after-smell might be very different from the odour signature, it is specific and temporally contiguous, thus providing the means to prolong the neural representation of the stimulus itself.

To investigate the logic of olfactory transformation and learning in the mushroom body, we constructed an MB neural network model based on the known connectivity in the insect brain. We showed that the model can process experimentally acquired input data and produce realistic KC response patterns. Our analysis suggests that the mushroom bodies enhance olfactory discrimination ability and stabilise the olfactory after-image, effectively prolonging the stimulus signature after odour offset.

Finally, we implemented a learning rule to modulate MB output neurons firing rate based on associative learning. We verified the model's predictions with behavioural measurements on real honey bees subjected to different learning protocols. The coherence between measured and predicted behavioural scores suggested that the rules behind this neural model - *i.e.* random connectivity, feedback inhibition, and MBON plasticity - are sufficient to generate relevant predictions for associative learning upon different learning protocols. In addition, by testing the model against physiological recordings of different stimulations, we showed that the model's predictions are robust to noise and biological variability.

Because the model incorporates not only neural assumptions pertaining to the honey bee olfactory system but also to the fruit fly and locust olfactory systems, similar principles may guide odour signal transformation at the level of the MB in appetitive associative learning across insects. This generality does not apply, however, to the nature of odour reshaping by

local interneurons observed in the AL of bees, which seems to differ from that occurring in flies, thus highlighting the fact that convergence, but also differences, can characterise the functional architectures of olfactory systems in different insect species.

Methods

Experimental Model

Experiments were performed on honey bees *Apis mellifera* reared in outdoor hives at the experimental apiary of the Research Centre on Animal Cognition (CNRS, Toulouse, France) situated in the campus of the University Paul Sabatier. In all cases, honey bee foragers (>3-week old) were used. No institutional permission is required for experimental research on honeybees

Projection neurons labelling

Honey bee foragers were collected the day before the experiment at an artificial feeder, to which they were previously trained, and projection neurons were labelled for calcium imaging analysis as previously described **(Paoli et al., 2017; Sachse and Galizia, 2002)**. Shortly, bees were fixed in a 3D-printed holder with soft dental wax, antennae were blocked frontally with a drop of eicosane (Sigma Aldrich, CAS: 112-95-8). A small window was opened in the head cuticle, and glands and tracheas were displaced to expose the injection site. The tip of a borosilicate glass needle coated with Fura-2-dextran (Thermo Fisher Scientific Inc.) was inserted between the medial and lateral mushroom body calyces, where medial (m-ACTs) and lateral antenno-cerebral tracts (l-ACTs) cross. After dye injection, the head capsule was closed to prevent brain desiccation, and bees were fed *ad libitum* with a 50% sucrose/water solution. On the following day, antennal lobes were exposed to allow optical access, and the brain was covered in transparent two-component silicon (Kwik-Sil, WPI). Although the injection

529 procedure may result in variable levels of PN labelling, the reproducibility of response
530 amplitudes and the lack of labelling bias for specific glomeruli indicate that the loading
531 procedure is reproducible.

532 Calcium imaging analysis and signal processing

533 Undiluted solutions of 1-hexanol, 1-heptanol and peppermint oil (Sigma-Aldrich) were
534 delivered to the bees using an Arduino Uno®-controlled automated olfactometer **(Bestea et**
535 **al., 2022; Raiser et al., 2017)**. Odorants were alternated and presented 20 times on a 5/25
536 second ON/OFF configuration. Calcium imaging recordings were conducted with a straight
537 Leica SP8 scanning microscope (Leica Microsystems, Germany) equipped with a
538 SpectraPhysics InSight X3 multiphoton laser tuned at 780 nm for Fura-2 excitation. All images
539 were acquired with a water immersion 16x objective (Leica HC FLUOTAR 16x/0.6 IMM CORR,
540 Leica Microsystems, Germany), at 64x64 pixel resolution and ~127 Hz.
541 Calcium imaging data were analysed with custom-made MATLAB (MathWorks Inc.)
542 scripts. The baseline signal, calculated as the mean fluorescence during the one second
543 before stimulus onset, was used to calculate baseline-subtracted and normalised stimulus-
544 induced glomerular activity ($\Delta F/F$). The normalised activity was multiplied by -1 to display
545 excitatory/inhibitory responses as positive/negative relative changes ($-\Delta F/F$). Time series of
546 glomerular activity were averaged across stimulus repetitions for response profile clustering
547 analysis. Glomeruli were hand-selected based on a morphological and functional map.
548 Glomerular response profiles were calculated as the mean intensity of an area of 5-by-5 pixels
549 around the centre of the glomerulus across time. Stimulus representation stability (**Fig. 1E**)
550 was assessed with a Person's correlation analysis between vectors of the mean glomerular
551 response of different trials. Glomerular response vectors' stability was calculated before,
552 during and after olfactory stimulation.

553 ## Mushroom Body Modelling

554 We used Matlab R2018a to investigate how the recorded PN activity would affect KC
555 responses of a MB network model.

556 ### Projection neurons to Kenyon cells connectivity

557 Real projection neurons' activity acquired *via* calcium imaging analysis provided the input
558 to a simple model of the mushroom body neural circuits. For each experimentally measured
559 honey bee, approx. 26 projection neurons (this number depends on the number of detected
560 glomeruli in the relative calcium imaging experiment) converge onto 1000 modelled KCs.
561 Connections between PNs and KCs were modelled as pseudo-random, with each KC receiving
562 connections from approx. 8 PNs (30% of the input PN population), as observed in bees
563 **(Szyszka et al., 2005)** and flies **(Ashok Litwin-Kumar et al., 2017; Caron et al., 2013)**. PN-
564 to-KC connections were assumed to be binary: either 0 (not connected), or 1 (connected), and
565 the connectivity scheme is stable in a given MB model and not subject to plastic changes. This
566 was implemented as a logic connectivity matrix (*W_PN_to_KC*) of size *number_of_PNs* ×
567 *number_of_KCs*. Experimental PNs activity (*PNactivity*) was resampled at 20 Hz for modelling
568 analysis (50 ms temporal resolution) to match the 20-Hz oscillatory cycle detected in the MB
569 **(Cassenaer and Laurent, 2007; Laurent and Naraghi, 1994; Popov and Szyszka, 2020)**.
570 For every time step *t*, the integrated input to each KCs (*KCepsp*) was calculated as the matrix
571 product of the input neuron activity vector (*PNactivity*) and the logical connectivity matrix. This
572 integrated input of each KC is analogous to its excitatory post-synaptic potential (EPSP).

573 $KCepsp(t) = PNactivity(t) \times W_PN_to_KC.$

574 ### Winner-takes-it-all inhibitory feedback element

575 Whether a KC will fire an action potential depends not only on the sum of its input signals
576 but also on the inhibitory activity of the MB feedback neurons **(Rybak and Menzel, 1993;**
577 **Zwaka et al., 2018)**. These neurons act on the whole KC population, providing that the KCs

578 receiving the highest summed input will produce an action potential (AP). To account for such
579 effect, and based on known MB neurophysiology **(Honegger et al., 2011; Peng and Chittka,**
580 **2017; Turner et al., 2008)**, we imposed that only the 10% most active *KCepsp* (*i.e.* receiving
581 the strongest summed input) will fire an action potential.

582 *If KC(i)epsp(t) > 10th percentil of KCepsp(t), then KC(i)activity(t) = 1; else KC(i)activity(t)*
583 *= 0*

584 This outputs a binary vector of firing pattern across the whole KC population (*KCactivity*),
585 where ones correspond to action potential and zeroes to silent KC. This operation is repeated
586 for all epochs to obtain the time course of the activity of the KC population before, during and
587 after odour arrival. To ensure the robustness of the model and account for the variability of the
588 initial parameters, the MB simulation was run 10 times for each experimental AL input dataset.
589 The results were then averaged over the 10 MB network simulations.

590 KC-to-MBON model and learning-induced plasticity

591 Evidence in *Drosophila* and in the honey bee suggests that the default state of an
592 appetitive MBON - *i.e.* an MBON departing from an MB lobe innervated by a dopaminergic
593 neuron conveying reward information - is to be broadly responsive to neutral stimuli **(Okada**
594 **et al., 2007; Owald et al., 2015)**. Under the assumption that similar principles are highly
595 conserved among insects, we modelled an MBON receiving connections from all KCs and with
596 all connections having an initial synaptic weight = 1 to reflect a generalised odour tuning. This
597 provides a broadly-tuned MBON that responds equally to any pattern of KC activity. Upon
598 learning, MBON synapses that are repeatedly recruited are switched off (= 0). As a
599 consequence, a trained MBON retains a high AP probability in the presence of an unfamiliar
600 stimulus, but a lower one in response to the conditioned odorant (or to an odorant that is
601 represented by a similar KC population). Two parameters guide learning: a synaptic plasticity
602 threshold (*spt*) and a learning window. The variable *spt* defines the number of firing events
603 needed for a given KC to induce its output synaptic depression (*i.e.* KC(i)_to_MBON synaptic
604 weight switch from 1 to 0). For the learning tests, a *spt* value of 15 was adopted. This value

605 falls in the middle of the range tested in our simulations (from 1 to 40). It is stringent enough
606 to hinder plastic modulation of rarely recruited KCs, while still requiring repetitive activation
607 (*i.e.* a synapse must be active at least 750 ms during a 3-s learning window) before allowing
608 learning-induced plasticity.

609 The learning window provides a temporal restriction of such a learning rule, analogous
610 to the reward/US delivery window in an appetitive conditioning protocol. Different CS/US
611 contingencies were tested. Inter-stimulus intervals (ISI) of -2, 1 and 4 were used, where such
612 values indicate the onset of a 3-s US window with respect to the onset of a 5-s CS window.
613 Throughout the manuscript, we referred to the three learning protocols as *backward* (ISI = -2),
614 *early* (ISI = 1), and *delay* (ISI = 4). The training was modelled using the mean glomerular
615 responses to the first 5 stimulations of 1-hexanol or peppermint oil; memory retention was
616 tested against the next 5 stimulations of both odorants (one acting as the conditioned stimulus,
617 the other one as the novel odorant).

618 ## Odorant response profiles simulation

619 The response profile database (**Fig. 1F**) was repeatedly subsampled to generate 100
620 odorant response maps, each comprising 30 glomerular responses. The proportion of
621 response types (inhibitory, excitatory, non-responsive, *etc.*) was maintained constant and
622 equal to the mean proportions across the entire population to generate a batch of similar
623 glomerular response maps (representing perceptually similar odorants **(Guerrieri et al., 2005)**)
624 (**Fig. 4G**). Projection neurons (or KC) response vectors used for the Pearson correlation
625 analysis are constituted by the average response for each PN (or KC) during olfactory
626 stimulation (t = 1 to 4 s).

627 ## Proboscis extension response latency

628 Bees were collected in the afternoon at the institute's outdoor beehives, kept in custom-
629 printed plastic cages in groups of 16 individuals, and provided with 240 microliters of 50%

630 sugar/water solution (an average of 15 μl for each individual). On the next morning, they were
631 harnessed in plastic tubes, blocked in place with tape, and fed 3 μl of sugar solution. Three
632 hours later, they were exposed to an absolute olfactory conditioning protocol **(Villar et al.,**
633 **2020)**. During conditioning, bees were placed in front of the odour delivery device (the same
634 one used for the calcium imaging analysis) and exposed to clean air for 15 s (familiarisation
635 phase), to the odorant for 5 s, and to clean air again for another 20 s. Three different intervals
636 were selected for delivering the sugar reward: either from 2 s before odour onset to 1 s after
637 (*backward conditioning*), from 1 to 4 s from odour onset (*early conditioning*) or from 4 to 7 s
638 from odour onset (*delay conditioning*). Bees were exposed to four rewarded trials, with a 10-
639 minute inter-trial-interval. Memory was tested 1 hour after the last conditioning trial. During the
640 memory test, videos were acquired with a commercial video camera at 30 fps. A LED
641 connected to the odour delivery device and in synch with the olfactory stimulation was used
642 as a marker for the starting timepoint for the measurement of proboscis extension latency.
643 Peppermint oil and 1-hexanol were used as olfactory stimuli. They were used non-diluted and
644 their role as conditioned stimulus (CS) or novel odorant (NOd) was balanced between bees.
645 During the test, half of the bees were exposed first to the CS and then to the NOd, while the
646 remaining half was tested in the opposite order. A 50% sugar/water solution (w/w) was used
647 as unconditioned stimulus (US).

648 ## Statistical Analysis

649 For MBON learning simulations, a total of 16 MB networks were generated and trained
650 with the PN response profiles to 1-hexanol (n = 8) or peppermint oil (n = 8). After training, each
651 MBON was tested against the response profiles of the CS and of the novel odorant to assess
652 AP firing probability to the learned and the unfamiliar stimulus. For each simulated MBON, 5
653 memory tests against the 5 repetitions of the CS and of the NOd were performed. To quantify
654 stimulus response to the conditioned/novel stimulus, the mean firing probability during the
655 time-window of stimulus arrival was calculated. The difference between the responses to the

CS and to the NOd was tested with a Kruskal-Wallis statistical test (**Fig. 5C**). The latency of MBON response to the CS was calculated as the latency to reach the 90% of minimal firing probability upon stimulation. The difference in latency between protocols was tested with a Kruskal-Wallis test; the difference in latency variance was assessed with a Barlett's test (**Fig. 5D**).

Proboscis extension response was used to assess memory retention 1 h after the last absolute conditioning trial. Conditioned stimulus specificity was tested with a McNemar test. The latency of CS-specific PER was measured as the first frame after stimulus onset, where the proboscis trespasses the imaginary line between the open mandibles (**Fig. 4E**). Differences between response latencies after early and delay conditioning were assessed with a Kruskal-Wallis test as well as with Barlett's test for difference in variance among datasets (**Fig. 4F**).

Bibliography

Adam, E., Hansson, B. S. and Knaden, M. (2022). Fast Learners: One Trial Olfactory Learning in Insects. *Front. Ecol. Evol.* **10**, 876596.

Amin, H. and Lin, A. C. (2019). Neuronal mechanisms underlying innate and learned olfactory processing in Drosophila. *Curr. Opin. insect Sci.* **36**, 9–17.

Ardin, P., Peng, F., Mangan, M., Lagogiannis, K. and Webb, B. (2016). Using an Insect Mushroom Body Circuit to Encode Route Memory in Complex Natural Environments. *PLoS Comput. Biol.* **12**, 1–22.

Ashok Litwin-Kumar, A., Decker Harris, K., Axel, R., Litwin-Kumar, A., Sompolinsky, H., Abbott, L. and Zuckerman, M. B. (2017). Optimal Degrees of Synaptic Connectivity. *Neuron* **93**, 1153-1164.e7.

Aso, Y., Sitaraman, D., Ichinose, T., Kaun, K. R., Vogt, K., Belliart-Guérin, G., Plaçais, P. Y., Robie, A. A., Yamagata, N., Schnaitmann, C., et al. (2014a). Mushroom body output neurons encode valence and guide memory-based action selection in Drosophila. *Elife* **3**, e04580.

Aso, Y., Hattori, D., Yu, Y., Johnston, R. M., Iyer, N. A., Ngo, T. T. B., Dionne, H., Abbott, L. F., Axel, R., Tanimoto, H., et al. (2014b). The neuronal architecture of the mushroom body provides a logic for associative learning. *Elife* **3**, e04577.

Bestea, L., Paoli, M., Arrufat, P., Ronsin, B., Carcaud, J., Sandoz, J.-C., Velarde, R., Giurfa, M. and de Brito Sanchez, M. G. (2022). The short neuropeptide F regulates appetitive but not aversive responsiveness in a social insect. *iScience* **25**, 103619.

Bitterman, M. E., Menzel, R., Fietz, A. and Schäfer, S. (1983). Classical conditioning of proboscis extension in honeybees (Apis mellifera). *J. Comp. Psychol.* **97**, 107–19.

Boisvert, M. J. and Sherry, D. F. (2006). Interval Timing by an Invertebrate, the Bumble Bee

Bombus impatiens. *Curr. Biol.* **16**, 1636–1640.
Buehlmann, C., Wozniak, B., Goulard, R., Webb, B., Graham, P. and Niven, J. E. (2020). Mushroom Bodies Are Required for Learned Visual Navigation, but Not for Innate Visual Behavior, in Ants. *Curr. Biol.* **30**, 3438-3443.e2.
Burke, C. J., Huetteroth, W., Owald, D., Perisse, E., Krashes, M. J., Das, G., Gohl, D., Silies, M., Certel, S. and Waddell, S. (2012). Layered reward signalling through octopamine and dopamine in Drosophila. *Nature* **492**, 433–7.
Caron, S. J. C., Ruta, V., Abbott, L. F. and Axel, R. (2013). Random convergence of olfactory inputs in the Drosophila mushroom body. *Nature* **497**, 113–7.
Cassenaer, S. and Laurent, G. (2007). Hebbian STDP in mushroom bodies facilitates the synchronous flow of olfactory information in locusts. *Nature* **448**, 709–713.
Chen, X., Ginoux, F., Carbo-Tano, M., Mora, T., Walczak, A. M. and Wyart, C. (2023). Granger causality analysis for calcium transients in neuronal networks, challenges and improvements. *Elife* 1–25.
Chou, Y.-H., Spletter, M. L., Yaksi, E., Leong, J. C. S., Wilson, R. I. and Luo, L. (2010). Diversity and Wiring Variability of Olfactory Local Interneurons in the Drosophila Antennal Lobe. *Nat. Neurosci.* **13**, 439–449.
Cognigni, P., Felsenberg, J. and Waddell, S. (2018). Do the right thing: neural network mechanisms of memory formation, expression and update in Drosophila. *Curr. Opin. Neurobiol.* **49**, 51–58.
Cohn, R., Morantte, I. and Ruta, V. (2015). Coordinated and Compartmentalized Neuromodulation Shapes Sensory Processing in Drosophila. *Cell* **163**, 1742–1755.
Deisig, N., Lachnit, H., Giurfa, M. and Hellstern, F. (2001). Configural Olfactory Learning in Honeybees: Negative and Positive Patterning Discrimination. *Learn. Mem.* **8**, 70.
Devaud, J.-M., Papouin, T., Carcaud, J., Sandoz, J.-C., Grünewald, B. and Giurfa, M. (2015). Neural substrate for higher-order learning in an insect: Mushroom bodies are necessary for configural discriminations. *Proc. Natl. Acad. Sci.* **112**, E5854–E5862.
Domjan, M. (2015). Classical conditioning: Foundations. In *The principles of learning and behavior* (ed. Domjan, M.), pp. 84–85. Stamford: Cengage Learning.
Dylla, K. V., Galili, D. S., Szyszka, P. and Lüdke, A. (2013). Trace conditioning in insects-keep the trace! *Front. Physiol.* **4 AUG**, 1–12.
Eschbach, C., Fushiki, A., Winding, M., Schneider-Mizell, C. M., Shao, M., Arruda, R., Eichler, K., Valdes-Aleman, J., Ohyama, T., Thum, A. S., et al. (2020). Recurrent architecture for adaptive regulation of learning in the insect brain. *Nat. Neurosci. 2020 234* **23**, 544–555.
Felsenberg, J., Plath, J. A., Lorang, S., Morgenstern, L. and Eisenhardt, D. (2014). Short- and long-term memories formed upon backward conditioning in honeybees (Apis mellifera). *Learn. Mem.* **21**, 37–45.
Finelli, L. A., Haney, S., Bazhenov, M., Stopfer, M. and Sejnowski, T. J. (2008). Synaptic learning rules and sparse coding in a model sensory system. *PLoS Comput. Biol.* **4**,.
Flanagan, D. and Mercer, A. R. (1989). An atlas and 3-D reconstruction of the antennal lobes in the worker honey bee, Apis mellifera L. (Hymenoptera : Apidae). *Int. J. Insect Morphol. Embryol.* **18**, 145–159.
Galili, D. S., Lüdke, A., Galizia, C. G., Szyszka, P. and Tanimoto, H. (2011). Olfactory trace conditioning in Drosophila. *J. Neurosci.* **31**, 7240–7248.
Galizia, C. G. (2014). Olfactory coding in the insect brain: data and conjectures. *Eur. J. Neurosci.* **39**, 1784–1795.
Galizia, C. G., Sachse, S., Rappert, A. and Menzel, R. (1999). The glomerular code for odor representation is species specific in the honeybee Apis mellifera. *Nat. Neurosci.* **2**, 473–8.
Ganeshina, O. and Menzel, R. (2001). GABA-Immunoreactive Neurons in the Mushroom Bodies of the Honeybee: An Electron Microscopic Study Indexing terms: GABA; postembedding EM-immunocytochemistry; microcircuits. *J. Comp. Neurol* **437**, 335–349.
Girardin, C. C., Kreissl, S. and Galizia, C. G. (2013). Inhibitory connections in the honeybee antennal lobe are spatially patchy. *J. Neurophysiol.* **109**, 332–343.

Giurfa, M. (2007). Behavioral and neural analysis of associative learning in the honeybee: a taste from the magic well. *J. Comp. Physiol. A 2007 1938* **193**, 801–824.

Giurfa, M. (2015). Learning and cognition in insects. *Wiley Interdiscip. Rev. Cogn. Sci.* **6**, 383–395.

Giurfa, M. and Sandoz, J.-C. (2012). Invertebrate learning and memory: Fifty years of olfactory conditioning of the proboscis extension response in honeybees. *Learn. Mem.* **19**, 54–66.

Gkanias, E., McCurdy, L. Y., Nitabach, M. N. and Webb, B. (2022). An incentive circuit for memory dynamics in the mushroom body of Drosophila melanogaster. *Elife* **11**,.

Grünewald, B. (1999). Morphology of feedback neurons in the mushroom body of the honeybee, Apis mellifera. *J. Comp. Neurol.* **404**, 114–26.

Guerrieri, F., Schubert, M., Sandoz, J. C. and Giurfa, M. (2005). Perceptual and neural olfactory similarity in honeybees. *PLoS Biol.* **3**, 0718–0732.

Hammer, M. (1993). An identified neuron mediates the unconditioned stimulus in associative olfactory learning in honeybees. *Nature* **366**, 59–63.

Heisenberg, M. (2003). Mushroom body memoir: From maps to models. *Nat. Rev. Neurosci.* **4**, 266–275.

Helassa, N., Zhang, X.-H., Conte, I., Scaringi, J., Esposito, E., Bradley, J., Carter, T., Ogden, D., Morad, M. and Török, K. (2015). Fast-Response Calmodulin-Based Fluorescent Indicators Reveal Rapid Intracellular Calcium Dynamics OPEN.

Hellstern, F., Malaka, R. and Hammer, M. (1998). Backward inhibitory learning in honeybees: A behavioral analysis of reinforcement processing. *Learn. Mem.* **4**, 429–444.

Hige, T., Aso, Y., Modi, M. N., Rubin, G. M. and Turner, G. C. (2015). Heterosynaptic Plasticity Underlies Aversive Olfactory Learning in Drosophila. *Neuron* **88**, 985–998.

Holland, P. C. (1980). CS-US interval as a determinant of the form of Pavlovian appetitive conditioned responses. *J. Exp. Psychol. Anim. Behav. Process.* **6**, 155–174.

Honegger, K. S., Campbell, R. A. A. and Turner, G. C. (2011). Cellular-Resolution Population Imaging Reveals Robust Sparse Coding in the Drosophila Mushroom Body. *J. Neurosci.* **31**, 11772–11785.

Huang, J., Zhang, W., Qiao, W., Hu, A. and Wang, Z. (2010). Functional Connectivity and Selective Odor Responses of Excitatory Local Interneurons in Drosophila Antennal Lobe. *Neuron* **67**, 1021–1033.

Huerta, R., Nowotny, T., García-Sanchez, M., Abarbanel, H. D. I. and Rabinovich, M. I. (2004). Learning classification in the olfactory system of insects. *Neural Comput.* **16**, 1601–1640.

Ito, I., Ong, R. C. Y., Raman, B. and Stopfer, M. (2008). Sparse odor representation and olfactory learning. *Nat. Neurosci.* **11**, 1177–1184.

Jeanne, J. M., Fişek, M. and Wilson, R. I. (2018). The organization of projections from olfactory glomeruli onto higher-order neurons. *Neuron* **98**, 1198-1213.e6.

Jefferis, G. S. X. E., Potter, C. J., Chan, A. M., Marin, E. C., Rohlfing, T., Maurer, C. R. and Luo, L. (2007). Comprehensive maps of Drosophila higher olfactory centers: spatially segregated fruit and pheromone representation. *Cell* **128**, 1187–1203.

Junek, S., Kludt, E., Wolf, F. and Schild, D. (2010). Olfactory Coding with Patterns of Response Latencies. *Neuron* **67**, 872–884.

Kim, B., Haney, S., Milan, A. P., Joshi, S., Aldworth, Z., Rulkov, N., Kim, A. T., Bazhenov, M. and Stopfer, M. A. (2023). Olfactory receptor neurons generate multiple response motifs, increasing coding space dimensionality. *Elife* **12**,.

Kirkpatrick, K. and Balsam, P. D. (2016). Associative learning and timing. *Curr. Opin. Behav. Sci.* **8**, 181–185.

Krofczik, S., Menzel, R. and Nawrot, M. P. (2009). Rapid odor processing in the honeybee antennal lobe network. *Front. Comput. Neurosci.* **2**, 9.

Laurent, G. and Davidowitz, H. (1994). Encoding of olfactory information with oscillating neural assemblies. *Science (80-.).* **265**, 1872–5.

Laurent, G. and Naraghi, M. (1994). Odorant-induced oscillations in the mushroom bodies of the locust. *J. Neurosci.* **14**, 2993–3004.

Le Moël, F. and Wystrach, A. (2020). Towards a multi-level understanding in insect navigation. *Curr. Opin. Insect Sci.* **42**, 110–117.

Le Moël, F., Stone, T., Lihoreau, M., Wystrach, A. and Webb, B. (2019). The central complex as a potential substrate for vector based navigation. *Front. Psychol.* **10**, 380097.

Lin, A. C., Bygrave, A. M., De Calignon, A., Lee, T. and Miesenböck, G. (2014). Sparse, decorrelated odor coding in the mushroom body enhances learned odor discrimination. *Nat. Neurosci.* **17**, 559–568.

Liu, C., Plaçais, P.-Y., Yamagata, N., Pfeiffer, B. D., Aso, Y., Friedrich, A. B., Siwanowicz, I., Rubin, G. M., Preat, T. and Tanimoto, H. (2012). A subset of dopamine neurons signals reward for odour memory in Drosophila. *Nature* **488**, 512–516.

Locatelli, F. F., Fernandez, P. C. and Smith, B. H. (2016). Learning about natural variation of odor mixtures enhances categorization in early olfactory processing. *J. Exp. Biol.* **219**, 2752–2762.

Lüdke, A., Raiser, G., Nehrkorn, J., Herz, A. V. M., Galizia, C. G. and Szyszka, P. (2018). Calcium in Kenyon cell somata as a substrate for an olfactory sensory memory in Drosophila. *Front. Cell. Neurosci.* **12**, 1–16.

Lyutova, R., Selcho, M., Pfeuffer, M., Segebarth, D., Habenstein, J., Rohwedder, A., Frantzmann, F., Wegener, C., Thum, A. S. and Pauls, D. (2019). Reward signaling in a recurrent circuit of dopaminergic neurons and peptidergic Kenyon cells. *Nat. Commun.* **10**,.

Malaka, R., Ragg, T. and Hammer, M. (1995). Kinetic models of odor transduction implemented as artificial neural networks. Simulations of complex response properties of honeybee olfactory neurons. *Biol. Cybern.* **73**, 195–207.

Menzel, R. (1999). Memory dynamics in the honeybee. *J. Comp. Physiol. A Sensory, Neural, Behav. Physiol.* **185**, 323–340.

Mertes, M., Carcaud, J. and Sandoz, J. C. (2021). Olfactory coding in the antennal lobe of the bumble bee Bombus terrestris. *Sci. Rep.* **11**, 1–14.

Mobbs, P. G. (1982). The brain of the honeybee Apis mellifera . I. The connections and spatial organization of the mushroom bodies. *Philos. Trans. R. Soc. London. B, Biol. Sci.* **298**, 309–354.

Moreaux, L. and Laurent, G. (2007). Estimating firing rates from calcium signals in locust projection neurons in vivo. *Front. Neural Circuits* **1**, 2.

Münch, D. and Galizia, C. G. (2016). DoOR 2.0 - Comprehensive mapping of Drosophila melanogaster odorant responses. *Sci. Rep.* **6**, 1–14.

Nouvian, M., Deisig, N., Reinhard, J. and Giurfa, M. (2018). Seasonality, alarm pheromone and serotonin: insights on the neurobiology of honeybee defence from winter bees. *Biol. Lett.* **14**,.

Okada, R., Rybak, J., Manz, G. and Menzel, R. (2007). Learning-related plasticity in PE1 and other mushroom body-extrinsic neurons in the honeybee brain. *J. Neurosci.* **27**, 11736–11747.

Olsen, S. R., Bhandawat, V. and Wilson, R. I. (2007). Excitatory interactions between olfactory processing channels in the Drosophila antennal lobe. *Neuron* **54**, 89–103.

Olshausen, B. A. and Field, D. J. (2004). Sparse coding of sensory inputs. *Curr. Opin. Neurobiol.* **14**, 481–487.

Owald, D., Felsenberg, J., Talbot, C. B., Das, G., Perisse, E., Huetteroth, W. and Waddell, S. (2015). Activity of defined mushroom body output neurons underlies learned olfactory behavior in Drosophila. *Neuron* **86**, 417–427.

Paoli, M. and Galizia, G. C. (2021). Olfactory coding in honeybees. *Cell Tissue Res.* **383**, 35–58.

Paoli, M. and Haase, A. (2018). In Vivo Two-Photon Imaging of the Olfactory System in Insects. In *Methods in molecular biology (Clifton, N.J.)*, pp. 179–219. Methods Mol Biol.

Paoli, M., Weisz, N., Antolini, R. and Haase, A. (2016). Spatially resolved time-frequency analysis of odour coding in the insect antennal lobe. *Eur. J. Neurosci.* **44**, 2387–2395.

Paoli, M., Andrione, M. and Haase, A. (2017). Imaging Techniques in Insects. In *Lateralized Brain Functions: Methods in Human and Non-Human Species* (ed. Rogers, L. J.) and

Vallortigara, G.), pp. 471–519. New York, NY: Springer New York.
Paoli, M., Albi, A., Zanon, M., Zanini, D., Antolini, R. and Haase, A. (2018). Neuronal response latencies encode first odor identity information across subjects. *J. Neurosci.* **38**, 9240 –9251.
Paoli, M., Macri, C. and Giurfa, M. (2023a). A cognitive account of trace conditioning in insects. *Curr. Opin. Insect Sci.* **57**, 101034.
Paoli, M., Antonacci, Y., Albi, A., Faes, L. and Haase, A. (2023b). Granger Causality Analysis of Transient Calcium Dynamics in the Honey Bee Antennal Lobe Network. *Insects 2023, Vol. 14, Page 539* **14**, 539.
Papadopoulou, M., Cassenaer, S., Nowotny, T. and Laurent, G. (2011). Normalization for sparse encoding of odours by a wide-field interneurons. *Science (80-.).* **332**, 721–725.
Patterson, M. A., Lagier, S. and Carleton, A. (2013). Odor representations in the olfactory bulb evolve after the first breath and persist as an odor afterimage. *Proc. Natl. Acad. Sci. U. S. A.* **110**,.
Pavlov, I. P. (1927). *Conditioned Reflexes: an Investigation of the Physiological Activity of the Cerebral Cortex*. (ed. Dr. G. V. Anrep) Oxford University Press.
Peng, F. and Chittka, L. (2017). A Simple Computational Model of the Bee Mushroom Body Can Explain Seemingly Complex Forms of Olfactory Learning and Memory. *Curr. Biol.* **27**, 224–230.
Perez-Orive, J., Mazor, O., Turner, G. C., Cassenaer, S., Wilson, R. I. and Laurent, G. (2002). Oscillations and sparsening of odor representations in the mushroom body. *Science (80-.).* **297**, 359–365.
Popov, T. and Szyszka, P. (2020). Alpha oscillations govern interhemispheric spike timing coordination in the honey bee brain. *Proc. R. Soc. B Biol. Sci.* **287**, 20200115.
Raiser, G., Galizia, C. G. and Szyszka, P. (2017). A High-Bandwidth Dual-Channel Olfactory Stimulator for Studying Temporal Sensitivity of Olfactory Processing. *Chem. Senses* **42**, 141–151.
Roussel, E., Carcaud, J., Combe, M., Giurfa, M. and Sandoz, J. C. (2014). Olfactory coding in the honeybee lateral horn. *Curr. Biol.* **24**, 561–567.
Rybak, J. and Menzel, R. (1993). Anatomy of the mushroom bodies in the honey bee brain: The neuronal connections of the alpha-lobe. *J. Comp. Neurol.* **334**, 444–465.
Sachse, S. and Galizia, C. G. (2002). Role of inhibition for temporal and spatial odor representation in olfactory output neurons: a calcium imaging study. *J. Neurophysiol.* **87**, 1106–17.
Sachse, S. and Galizia, C. G. (2003). The coding of odour-intensity in the honeybee antennal lobe: Local computation optimizes odour representation. *Eur. J. Neurosci.* **18**, 2119–2132.
Sachse, S., Rappert, A. and Galizia, C. G. (1999). The spatial representation of chemical structures in the antennal lobe of honeybees: Steps towards the olfactory code. *Eur. J. Neurosci.* **11**, 3970–3982.
Schäfer, S. and Bicker, G. (1986). Distribution of GABA-like immunoreactivity in the brain of the honeybee. *Neuroscience* **246**, 287–300.
Schmalz, F., el Jundi, B., Rössler, W. and Strube-Bloss, M. (2022). Categorizing Visual Information in Subpopulations of Honeybee Mushroom Body Output Neurons. *Front. Physiol.* **13**, 1–11.
Shang, Y., Claridge-Chang, A., Sjulson, L., Pypaert, M. and Miesenböck, G. (2007). Excitatory local circuits and their implications for olfactory processing in the fly antennal lobe. *Cell* **128**, 601–12.
Smith, D., Wessnitzer, J. and Webb, B. (2008). A model of associative learning in the mushroom body. *Biol. Cybern.* **99**, 89–103.
Springer, M. and Nawrot, M. P. (2021). A Mechanistic Model for Reward Prediction and Extinction Learning in the Fruit Fly. *eNeuro* **8**,.
Stopfer, M. (2014). Central processing in the mushroom bodies. *Curr. Opin. Insect Sci.* **6**, 99–103.
Strausfeld, N. J. (2002). Organization of the honey bee mushroom body: Representation of

the calyx within the vertical and gamma lobes. *J. Comp. Neurol.* **450**, 4–33.

Strube-Bloss, M. F. and Rössler, W. (2018). Multimodal integration and stimulus categorization in putative mushroom body output neurons of the honeybee. *R. Soc. Open Sci.* **5**, 171785.

Strutz, A., Soelter, J., Baschwitz, A., Farhan, A., Grabe, V., Rybak, J., Knaden, M., Schmuker, M., Hansson, B. S. and Sachse, S. (2014). Decoding odor quality and intensity in the Drosophila brain. *Elife* **3**, e04147.

Szyszka, P., Ditzen, M., Galkin, A., Galizia, C. G. and Menzel, R. (2005). Sparsening and temporal sharpening of olfactory representations in the honeybee mushroom bodies. *J. Neurophysiol.* **94**, 3303–3313.

Szyszka, P., Demmler, C., Oemisch, M., Sommer, L., Biergans, S., Birnbach, B., Silbering, A. F. and Galizia, C. G. (2011). Mind the gap: Olfactory trace conditioning in honeybees. *J. Neurosci.* **31**, 7229–7239.

Takeda, K. (1961). Classical conditioned response in the honey bee. *J. Insect Physiol.* **6**, 168–179.

Turner, G. C., Bazhenov, M. and Laurent, G. (2008). Olfactory representations by Drosophila mushroom body neurons. *J. Neurophysiol.* **99**, 734–46.

Villar, M. E., Marchal, P., Viola, H. and Giurfa, M. (2020). Redefining single-trial memories in the honeybee. *Cell Rep.* **30**, 2603-2613.e3.

Wilson, R. I., Turner, G. C. and Laurent, G. (2004). Transformation of Olfactory Drosophila Antennal Lobe. *Science (80-.).* **303**, 366–370.

Wystrach, A. (2023). Neurons from pre-motor areas to the Mushroom bodies can orchestrate latent visual learning in navigating insects. *bioRxiv* 2023.03.09.531867.

Yaksi, E. and Wilson, R. I. (2010). Electrical coupling between olfactory glomeruli. *Neuron* **67**, 1034–47.

Zwaka, H., Bartels, R., Grünewald, B. and Menzel, R. (2018). Neural organization of A3 mushroom body extrinsic neurons in the honeybee brain. *Front. Neuroanat.* **12**, 1–11.

Figures

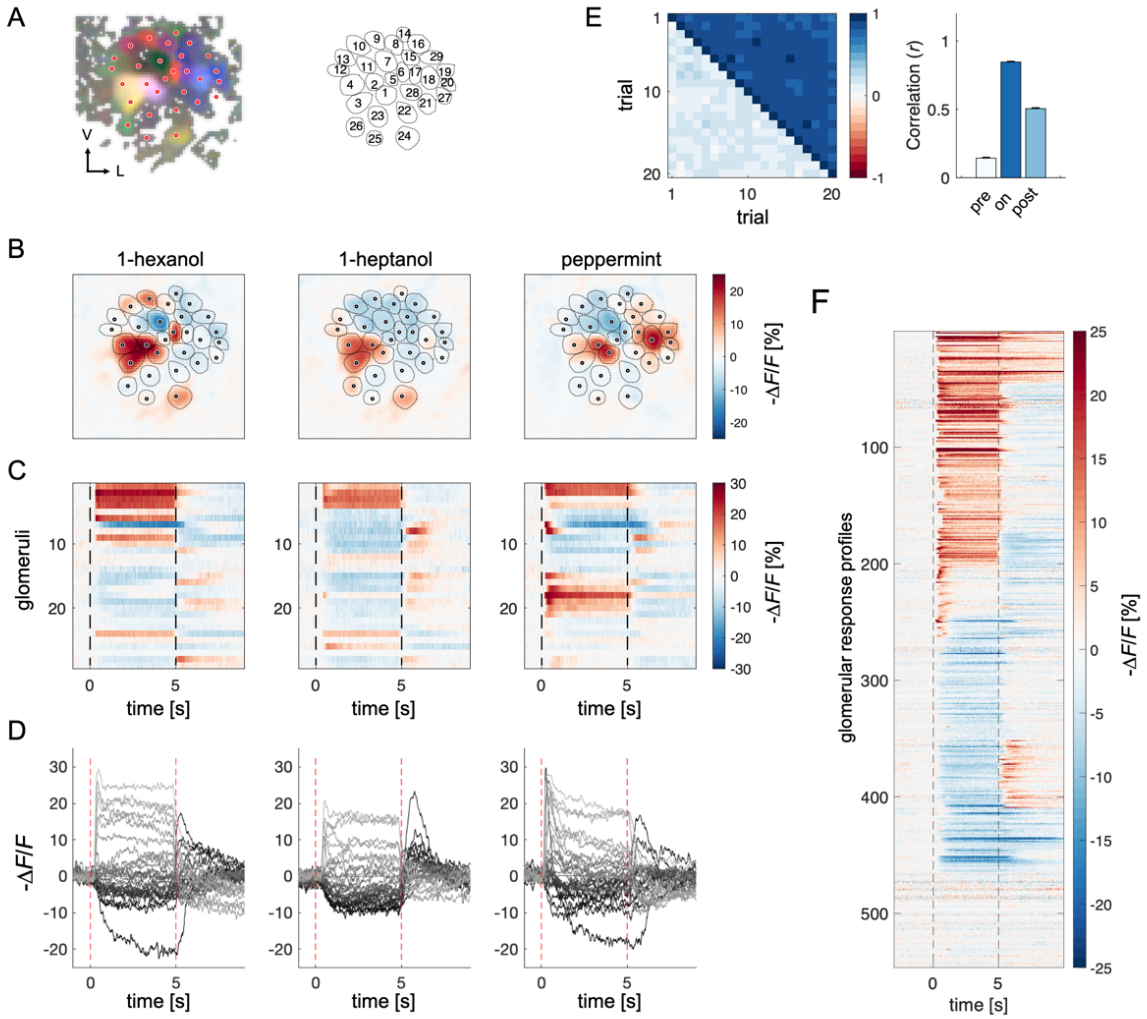

Figure 1. Projection Neurons Calcium Imaging Analysis
(A) For each AL, the response maps to all three odorants were overlaid to highlight glomerular structures. Glomeruli were hand-labelled for time-series extraction. V, ventral; L, lateral.
(B) Exemplary AL odorant responses during olfactory stimulation with three odorants. Colorbar indicates the relative change of activity during olfactory stimulation with respect to the pre-stimulus baseline. Circular areas indicate identified glomeruli according to **(A)**
(C,D) Temporal profiles of the glomerular regions identified in **(A)** for the three odorants. Each line in (**C**), labelled from 1 to 28, refers to the glomerular ID in (**A**). Temporal profiles represent the average activity of 20 stimulations. Dashed lines in (**C,D**) limit the begin and the end of the olfactory stimulation.
(E) Matrix of Pearson's correlations between pairs of glomerular response vectors across all repetitions. The upper right part of the matrix shows correlation scores among glomerular activity during olfactory stimulation (t = 1 to 4 s after odorant onset) across trials; the bottom left part shows correlation scores among glomerular activity before stimulation (t = -1 to 0 s) across trials. On the right, the mean (± s.e.m.) across-trial correlation before, during and after (t =6 to 9s) stimulation is shown.
(F) All glomerular responses from 8 ALs to 3 odorants were pooled together to provide an overview of the complexity of response profiles *(n* = 546*).*

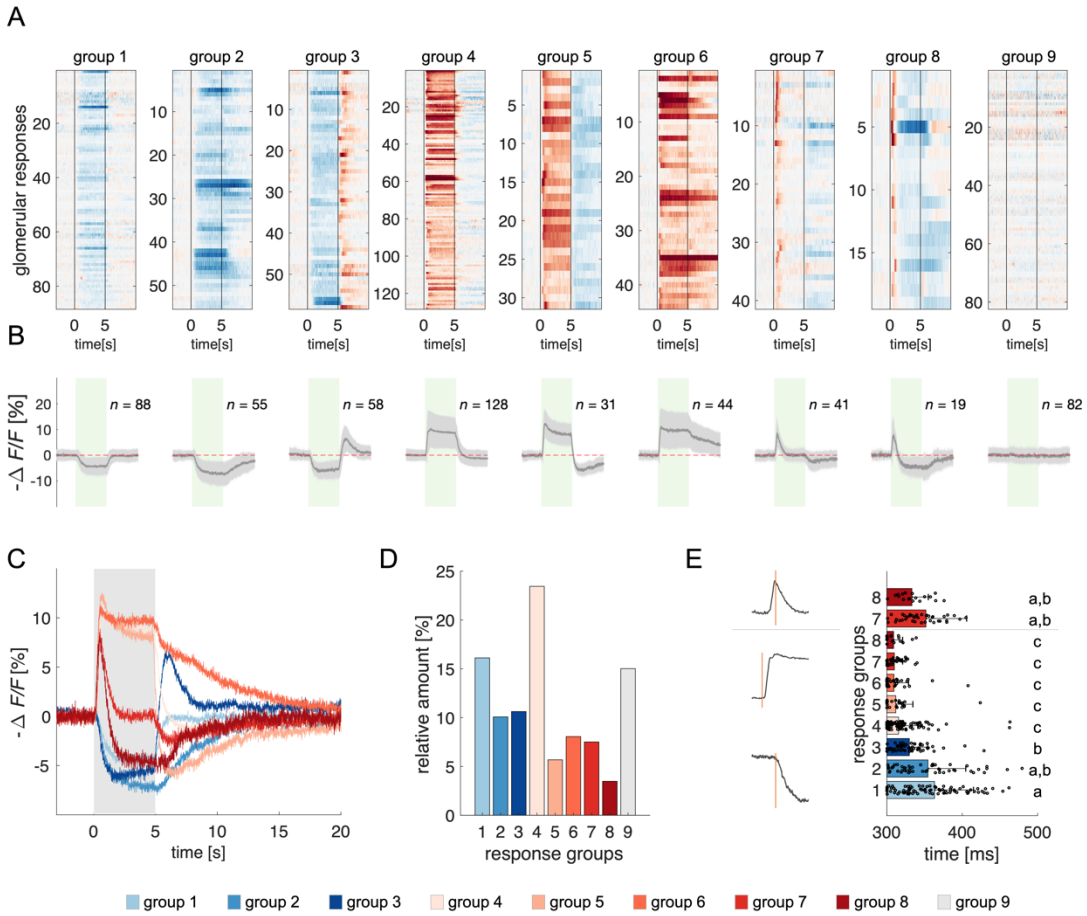

Figure 2. Clustering of Projection Neurons' Response Profiles
(A) All glomerular responses were clustered with supervision according to their activity (excitatory, inhibitory, non-responsive) during and after stimulus arrival.
(B) Mean ± s.e.m. of all curves of the relative groups in (**A**). The green patch indicates the stimulus delivery interval.
(C) Average curves of all response groups from (**B**) are superimposed. The grey patch indicates the stimulus delivery interval.
(D) Relative amount of all response categories.
(E) Latency of glomerular responses for excitatory and inhibitory profiles (groups 1 to 8). For groups 7 and 8, the latency of short excitatory response's termination was calculated. Letters refer to significative groups after Kruskal-Wallis statistical test and Tukey-Kramer correction. On the left side, exemplary traces of phasic and tonic excitatory responses and an inhibitory response are shown. The orange line indicates the latency of response onset or termination.

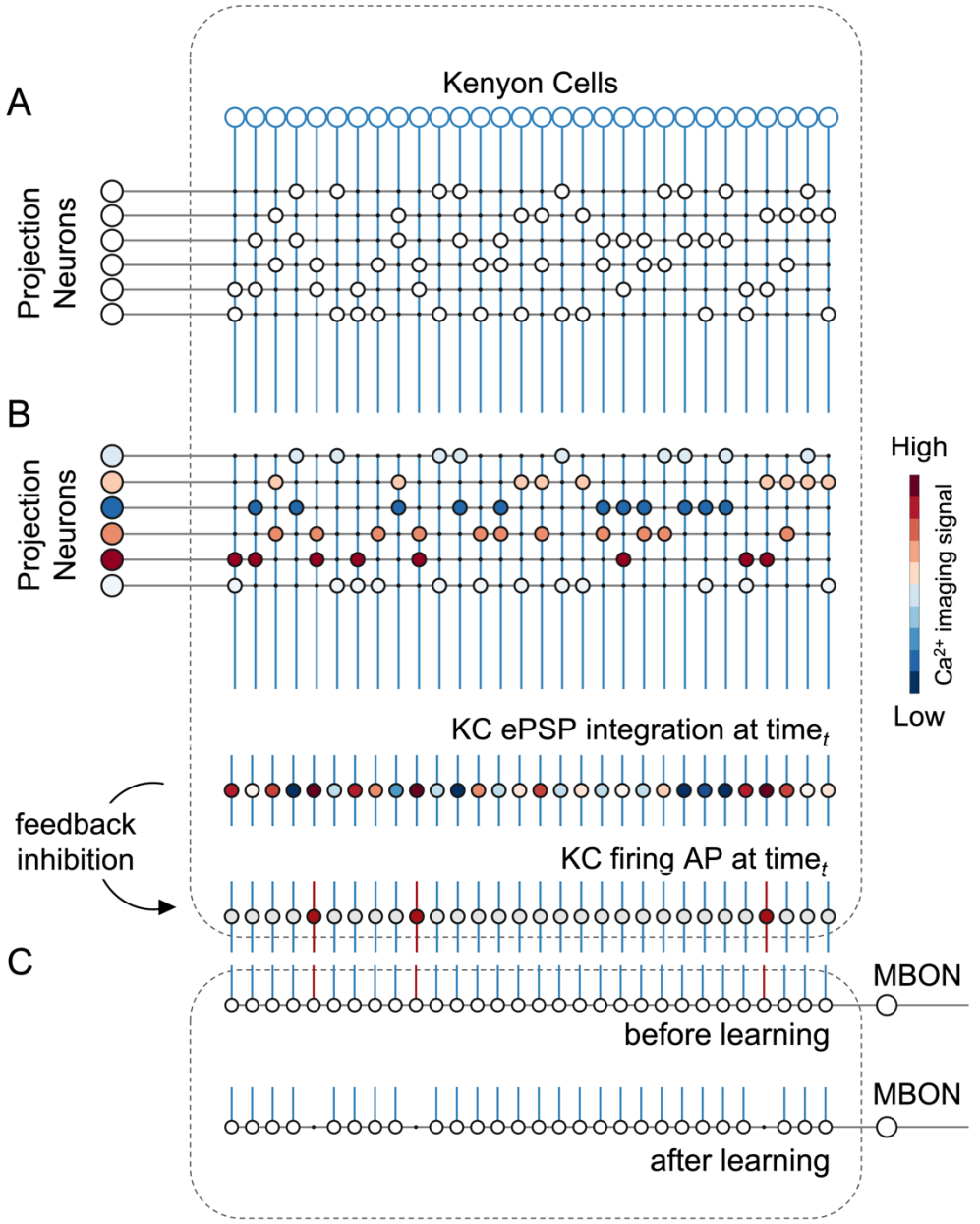

Figure 3. A Simple Neural Network Model for Olfactory Coding and Learning.
(A) The synaptic connectivity between AL PNs and KCs is built as a pseudorandom logic matrix where each column represents KC dendritic arborisation and each row PN axon terminals. Each KC receives synaptic contact – here represented as a white circle – from 30% of the PN population.
(B) For each timepoint *t* of a calcium imaging recording, the measured activity level for each glomerulus (represented by a PN in the model) is projected onto all its synaptic connections with the KC population. Each KC, *i.e.* each column in the scheme, integrates all excitatory post-synaptic potentials. Finally, recurrent inhibitory feedback is simulated by imposing that only the 10% most active KCs will generate an action potential (AP) (red cells), while all others remain silent (grey cells).
(C) A single appetitive MBON receiving input from all KCs was modelled. Based on a synaptic plasticity threshold parameter, all synapses from KCs to MBON that are activated with a

frequency greater than allowed by the defined threshold during the learning window will be switched off. This phenomenon results in a decrease AP probability in the modelled MBON upon stimulation with the learned stimulus. Abbreviations: action potential, AP; antennal lobe, AL; excitatory post-synaptic potential, ePSP; Kenyon cells, KC; mushroom body, MB; mushroom body output neuron, MBON; projection neurons, PN.

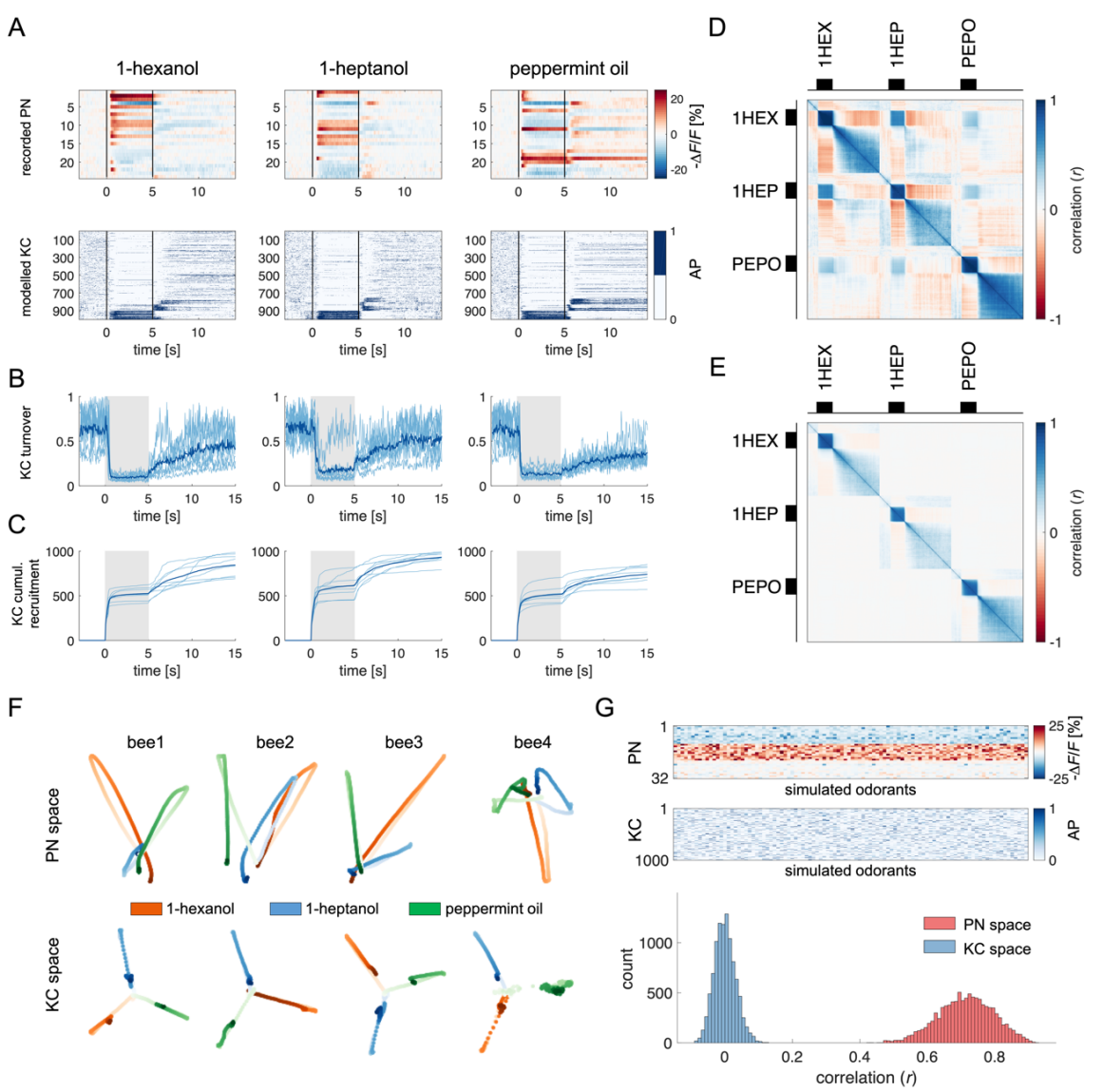

Figure 4. Olfactory Representation in Modelled Kenyon Cells
(A) The first row displays the recorded PN responses of one honey bee to three odorants. The second row shows the transformation of the PN activity operated by the model to simulate the activity of 1000 KCs. In each plot, KCs are ordered for response strength during the onset and offset to better visualise activity clusters.
(B) Turnover rate of recruited KCs across adjacent time points. Light blue traces refer to individual bees (mean of 10 MB simulations). Thick, dark blue traces indicate average curves across bees.
(C) Cumulative recruitment of KC shows two main recruitment events at stimulus onset and offset. To observe odorant-related KC recruitment dynamics, the cumulative sum was initiated at stimulus onset. Light blue traces refer to individual bees (mean of 10 MB simulations). Thick, dark blue traces indicate average curves across bees.
(D,E) Correlation matrix among time points of measured PN activity (**C**) and simulated KC activity (**E**). Mean responses to the three odorants were concatenated to allow observing within and across odorant correlations.
(F) PCA of odorants' trajectories in the measured PN space (top) and in the modelled KC space (bottom) for four exemplary bees. Trajectories comprise a 10-s interval, ranging from odour onset (t = 0 s, light) to 5 s after offset (t = 10 s, dark).
(G) The raster plot shows a set of 100 artificially combined glomerular responses (top), each simulating the neural representation of 100 similar odorants in the PN space. A second raster plot (middle) shows the representation of the same odorants in the modelled KC space. Note that

odorant representation was considered as the mean activity of PN (or KC) during stimulus arrival (0.5 to 5 s). The histogram shows the distributions of between-odorant correlations computed among all pairs of odour vectors in the PN and KC space. A significant difference between the two distributions was tested with a Student's *t* test ($p \approx 0$, $n = 4774$).

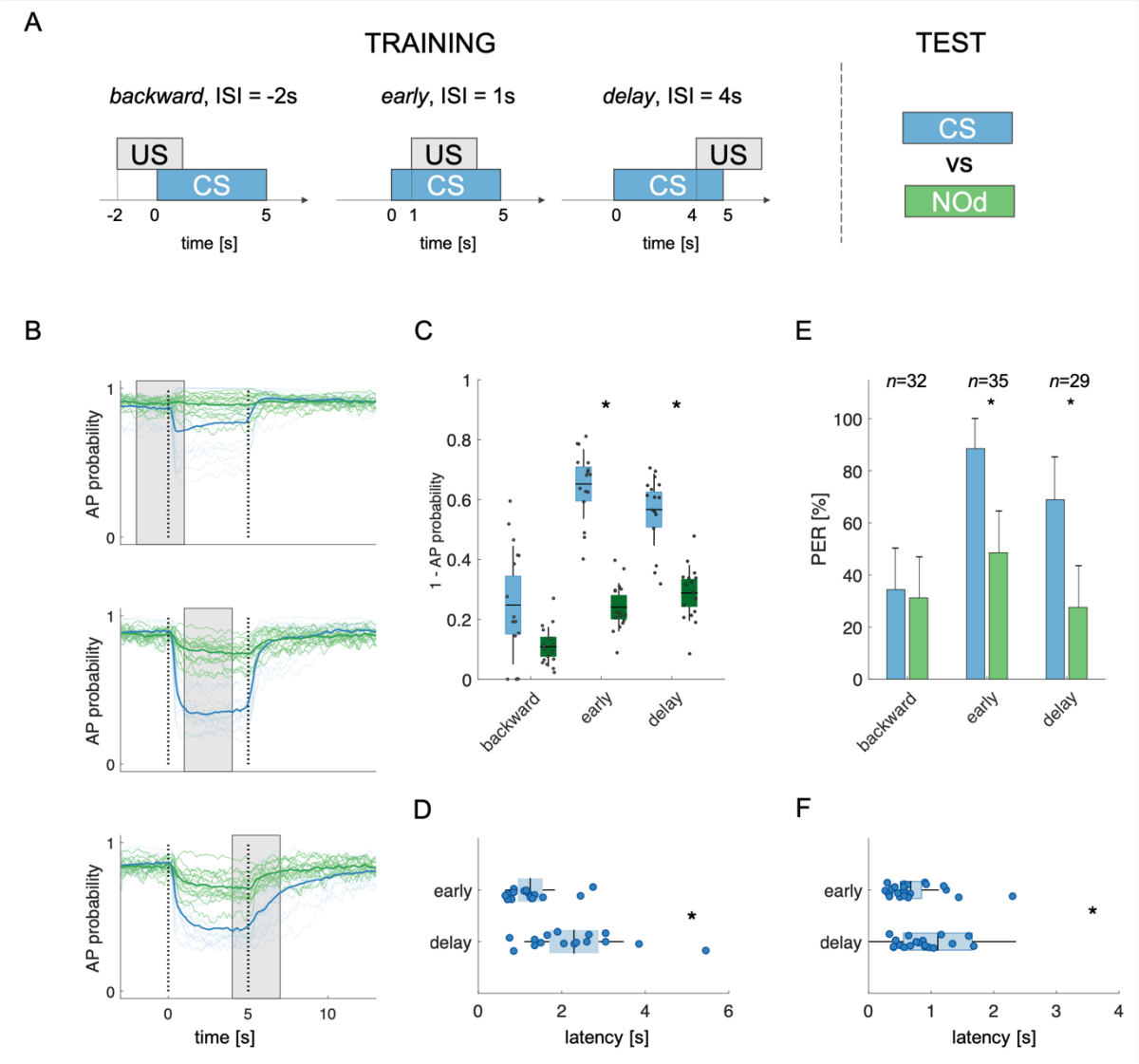

Figure 5. Modelled Mushroom Body Output Neuron Predicts Appetitive Behavior

(**A**) Three experimental protocols differing for CS/US inter stimulus interval (ISI) were used for training the model (**B-D**) and for behavioural measurements of the proboscis extension reflex conditioning (**E**,**F**). Trained simulated MBONs, as well as conditioned honey bees were tested against the CS (blue) and a novel odorant (NOd, green).

(**B**) Time course of action potential (AP) probability of a trained MBON upon stimulation with the CS (blue) or with the novel odorant (NOd, green). Olfactory learning was modelled according to *backward* (top), *early* (middle) and *delay* (bottom) CS/US contingencies. Glomerular responses for 8 bees to 1-hexanol and peppermint oil were used alternatively as CS and NOd. Data for responses to CS and NOd were pooled together (n = 16 traces for each condition. Blue traces, CS; green traces, NOd). The thick trace shows the average AP probability profile; dotted vertical lines delimit the stimulation interval; grey bar delimits the simulated learning window.

(**C**) Distribution of the mean values of traces in (**B**) during CS and NOd stimulation. Because appetitive learning produces a decrease in MBON firing rate, the complementary value of the probability fraction is used as a proxy for a learned appetitive response ($p_{backward}$ = 0.06; p_{early} = 1.41*10-6; p_{delay} = 1.04*10-5; Kruskal-Wallis statistical test; n = 16).

(**D**) Latency of 90% of minimal MBON activity in response to the CS+ for early and delay conditioning protocols (Kruskal-Wallis test for difference in distribution across protocols, p = 0.002; Barlett's test for variance difference across protocols, p = 0.0109).

1042 (**E**) Memory retention test of honey bees 1 h after absolute conditioning. Bars indicate the
1043 percentage of individuals showing proboscis extension reflex (PER) when presented with the
1044 conditioned or the novel odorant. Error bars indicate 95% confidence intervals. (Responses to the
1045 CS/NOd were compared with a McNemar test for binomial distribution; $p_{early} = 0.003$, $p_{delay} = 0.004$)
1046 (**F**) Latency of the PER to the conditioned stimulus at the 1 h memory retention test (Kruskal-Wallis
1047 test for difference in distribution across protocols, $p = 0.036$; Barlett's test for variance difference
1048 across protocols, $p = 5*10-6$; $n_{early} = 26$; $n_{delay} = 20$).
1049

1050 ## Supplementary Figures

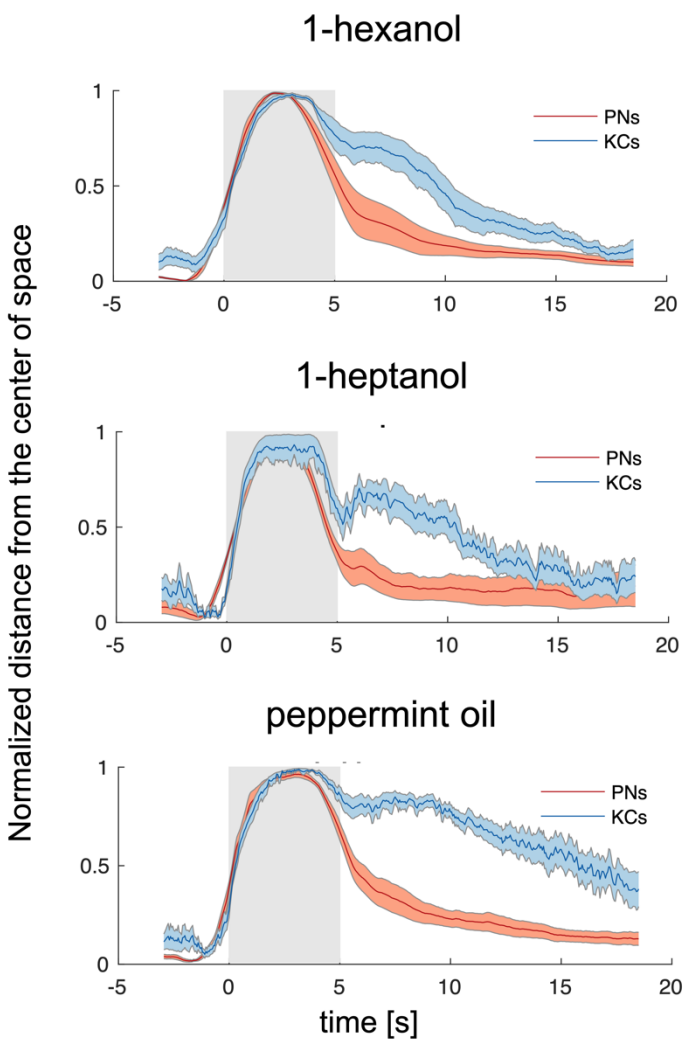

1051

1052 **Supplementary Figure S1. Odorant-Specific Activity Lasts Longer in the Kenyon Cells**
1053 **Space.**
1054 Time traces of the normalized Euclidean distance from the centre of coordinates (where the centre
1055 of coordinates was set to 0 and the maximum distance from it was set to 1) in the PN and KC space
1056 for the three odorants. This transformation allowed performing a direct comparison between the
1057 temporal dynamics of the representations of one odorant in the PN and KC space. Discriminability
1058 – that is distance from 0 – peaks during olfactory stimulation, but is maintained longer in the KC
1059 space. Notably, such long-lasting odorant-specific signature is not achieved by maintaining onset-
1060 recruited neurons activity for a longer period of time, but by recruiting two pools of KCs (both
1061 odorant-specific), one for the ON phase, and one during the OFF phase (see also Figure 4). Grey
1062 patches indicate stimulation windows. Traces represent mean ± s.e.m. of 8 animals (PN data, red)
1063 and relative MB simulations (KC data, blue).
1064

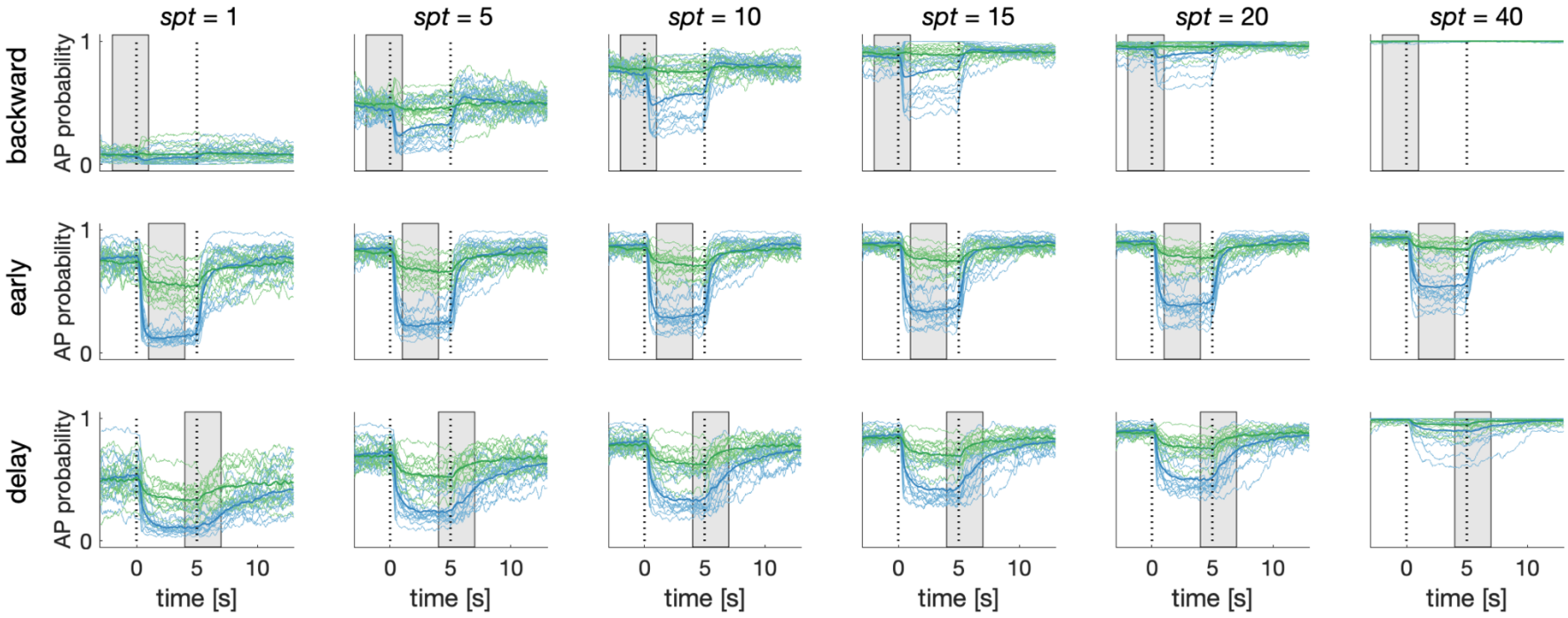

Supplementary Figure S2. Dependence of Simulated MBON Activity on Synaptic Plasticity Threshold. Synaptic plasticity threshold (*spt*) dictates how many times a KC-to-MBON synapse has to be recruited during the learning window before being switched off. The influence of *spt* on MBON learning was tested for all CS/US protocols. The extreme values of the parameters (*spt* = 1 and 40) indicate that a certain synapse should be recruited only once or 40 times before being turned off (note that to be activated 40 times in a 3-s learning window and with 20 Hz sampling rate, a synapse should fire for two entire seconds). With the exceptions of the extreme parameters, the MBON AP probability upon CS and NOd presentation is only weakly affected by *spt* value. Notably, small *spt* results in higher generalized learning, while a large *spt* require a stable KC signal for synapses to be modulated and produces weaker learning scores.